Master thesis

High Temperature Oxidation
of Si-Containing Steel

Song, Eun-Ju (宋恩周)

Computational Metallurgy

Graduate Institute of Ferrous Technology

Pohang University of Science and Technology

2011

Si 함유강의 고온산화 해석

High temperature Oxidation
of Si-Containing Steel

High Temperature Oxidation
of Si-Containing Steel

By

Song, Eun-Ju
Computational Metallurgy
Graduate Institute of Ferrous Technology
Pohang University of Science and Technology

A thesis submitted to the faculty of Pohang University of Science and Technology in partial fulfillments of the requirements for the degree of Master of Science in the Graduate Institute of Ferrous Technology (Computational Metallurgy)

Pohang, Korea
April 14th, 2011

Approved by

Prof. Bhadeshia, H.K.D.H.   Prof. Suh, Dong-Woo

_____   _____

Major Advisor   Co-Advisor

High Temperature Oxidation
of Si-Containing Steel

Song, Eun-Ju

This dissertation is submitted for the degree of Master of Science at the Graduate Institute of Ferrous Technology of Pohang University of Science and Technology. The research reported herein was approved by the committee of Thesis Appraisal.

April 14th, 2011

Thesis Review Committee
Chairman: Prof. Bhadeshia, H.K.D.H.
(Signature)_____
Member: Prof. Suh, Dong-Woo
(Signature)_____
Member: Prof. Lee, Jae Sang
(Signature)_____

MFT   Song, Eun-Ju
20091048   High temperature oxidation of Si containing steel
             Computational Metallurgy 2011
             Advisor: Prof. Bhadeshia, H.K.D.H
             Text in English

Abstract

Red-scale is caused by the residual primary scale prior to hot rolling. In silicon-containing steel, during reheating, liquid fayalite (Fe_2SiO_4) forms and makes descaling difficult, thus it produces the red-scale. The aim of this study is to predict the formation of oxides so as to reduce red-scale formation and optimize the silicon concentration in steel.

The formation of oxides on Fe – 0.1 C – (0 ~ 13) Si wt% steel at high temperature in air has been studied. In air, the formation energies of FeO, Fe_2SiO_4 and SiO_2 are negative, thus those oxides can in practice form spontaneously. The most stable phase is SiO_2 in air. However, FeO, SiO_2 and Fe_2SiO_4 cannot exist in equilibrium at the single oxygen pressure at high temperatures because Fe_2SiO_4 is more stable than SiO_2 for the given condition.
The mechanism for SiO_2 and Fe_2SiO_4 growth based on the diffusion of silicon in steel is suggested and the growth rates of SiO_2, Fe_2SiO_4 have been calculated according to that mechanism. The calculated growth rates of SiO_2, Fe_2SiO_4 and FeO at 1000 °C are, $1.62 \times 10^{-7}\ \mu m^2\ s^{-1}$, $2.269 \times 10^{-6}\ \mu m^2\ s^{-1}$ and $0.12\ \mu m^2\ s^{-1}$, respectively for the relevant conditions. FeO grows much faster than Fe_2SiO_4 and Fe_2SiO_4 grow faster than SiO_2. The volume fraction of each phase has been predicted according to the calculated growth rate.

The oxides on Fe – 0.1 C – 1 Si wt% steel at 1000 °C and 1250 °C in air have been investigated with microscopy. Also, the effects of nickel and aluminum are investigated. The addition of nickel in Si-containing steel makes the steel/oxide interface uneven. However, no significant effect was found with the addition of aluminum.

Nomenclature

a_{Si}	Activity of silicon which reference state is diamond Si
a_{Fe}	Activity of iron which reference state is BCC ferrite
A_{FeO}	Area of FeO on the steel surface
$A_{\text{Fe}_2\text{SiO}_4}$	Area of Fe_2SiO_4 on the steel surface
A_{SiO_2}	Area of SiO_2 on the steel surface
BCC	Body centered cubic
D_{Fe}^{FeO}	Diffusivity of iron in FeO
D_{O}^{FeO}	Diffusivity of oxygen in FeO
D_{Si}^{α}	Diffusivity of silicon in ferrite
D_{Si}^{γ}	Diffusivity of silicon in austenite
FCC	Faced centered cubic
Fe_3C	Cementite
FeO	Wüstite
Fe_2O_3	Hematite
Fe_2SiO	Fayalite
Fe_3O_4	Magnetite
k'_{FeO}	Parabolic growth rate of FeO between steel/Fe_3O_4
k'_{FeO}	Parabolic growth rate of FeO between steel/O_2
k_{FeO}^{O}	Parabolic growth rate of FeO based on the migration of O
$k_{\text{Fe}_2\text{SiO}_4}$	Parabolic growth rate of Fe_2SiO_4

k_{SO_2}	Parabolic growth rate of SiO_2
N_{FeO}	Nucleation sites per area of FeO on the steel surface
$N_{Fe_2SiO_4}$	Nucleation sites per area of Fe_2SiO_4 on the steel surface
N_{SiO_2}	Nucleation sites per area of SiO_2 on the steel surface
P_{O_2}	Partial pressure of oxygen
r^*	Critical radius for nucleation forming
z	Thickness of the oxide
ΔG	Gibbs free energy
ΔG^0	Standard Gibbs free energy
ΔG^*	Maximum excess free energy for nucleation forming
γ_o	Surface energy of the oxide
γ_{so}	Interface energy between the steel and oxide

Contents

1 Introduction

Steels are usually combinations of Body-Centered-Cubic (BCC) ferrite, Face-Centered-Cubic (FCC) austenite and orthorhombic cementite (Fe_3C) phases as seen in Fig. 1.1. The alloying element and thermo-mechanical processing of the steel determine the fractions of each phase and the details of the microstructure. The phases and microstructure can determine properties such as strength, toughness and hardenability.

Among alloying elements, silicon plays several important roles. First, it prevents cementite precipitation from austenite. There is a particular mixture of phases in steels which has led to dramatic developments in their application, which is dubbed carbide-free bainite (Matsumura *et al.*, 1987; Jacques *et al.*, 1999; Caballero *et al.*, 2001; De Cooman, 2004; De Cooman, 2007). It is a combination of fine ferrite plates and carbon-enriched retained austenite. The latter phase is commonly unstable at room temperature, but is made stable by preventing cementite precipitation with a silicon addition to the steel. The austenite is then able to retain carbon in solid solution, allowing it to stay untransformed to room temperature. For precipitation of cementite at low temperatures, it must maintain the silicon concentration of the parent phase; since the solubility of silicon in cementite is almost zero, the entrapping of silicon is thought to dramatically decrease the driving force for precipitation (Ghosh and Olson, 2002; Bhadeshia
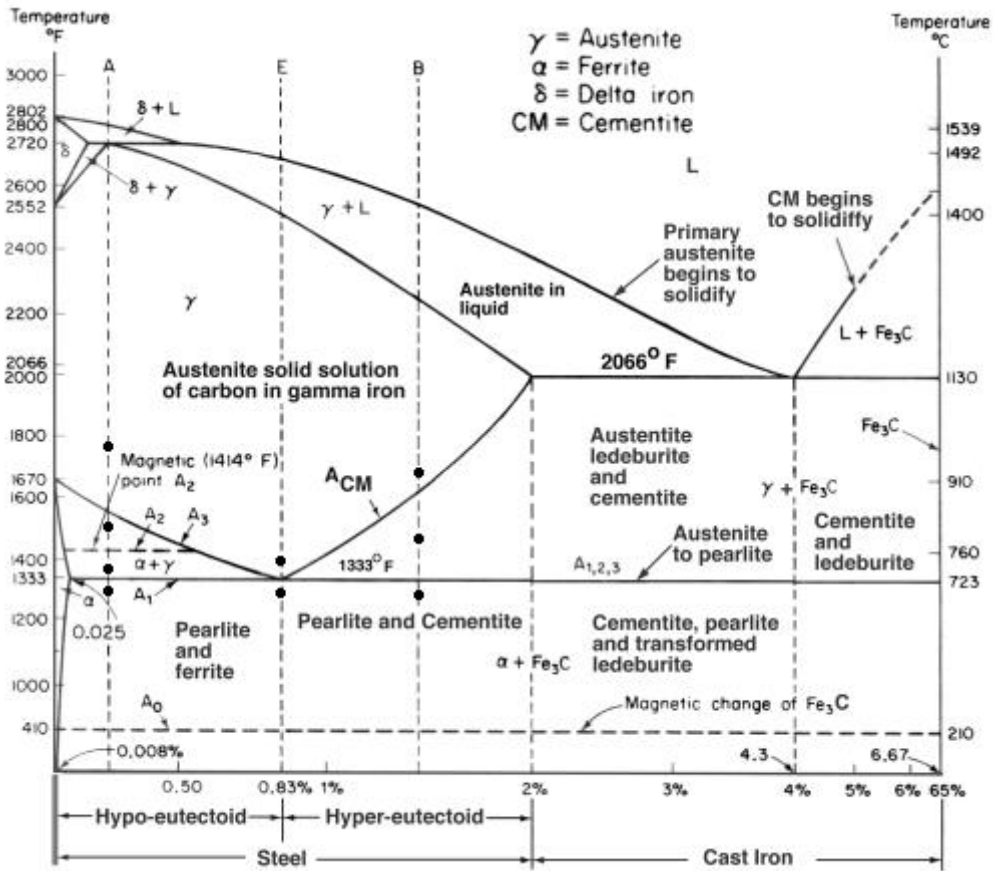
Fig. 1.1 An iron-carbon metastable equilibrium diagram (Pollack, 1977).

.

Secondly, silicon itself has a solid solution hardening effect and it does not decrease ductility within the limits used. It is also added to improve the electrical resistance of steels used in the manufacture of components such as transformers (De Cooman, 2007).

However, it is necessary to optimize the silicon concentration in order to avoid

the formation of an adherent red-scale on the surface of the steel. It is found that the red-scale is powdered-αFe_2O_3, and is difficult to remove, thus reducing aesthetic appearance and commercial value of the steel product. Moreover, the resulting embedded oxide defects on the surface of the steel cause subsequent problems during any coating process (Fukagawa *et al.*, 1994; Raman, 2006).

Conventional hot-rolling comprises three major steps, which are slab reheating, hot rolling and coiling. During the reheating process, steel slabs, each weighing about 3 t, are heated to about 1200 °C and a thick layer of oxide scale, designated the primary scale forms. High temperature oxidation results in the formation of an oxide layer on the metal. The oxide layer, whose thickness is above 3000 Å, is called the "scale" and a thinner one is designated 'film'. A hydraulic descaler near the exit of the reheat furnace removes the scale but if some persists prior to the rolling process, it may become embedded. If this remaining scale is fractured by rolling, the red-scale is formed whether the steel contains silicon or not. However, for the silicon-added steel, descaling is more difficult due to the appearance of fayalite (Fe_2SiO_4) at the scale/steel interface (Fukagawa *et al.*, 1994; Okada *et al.*, 1995; Raman, 2006), as discussed in detail in the next chapter. It is required therefore to improve the descalability in order to detach the red-scale and some methods have been reported in accordance with this need. The removal of Ni (< 0.02 wt%) reduces the problem (Fukagawa *et al.*, 1996; Asai *et al.*, 1997). A small concentration of P (> 0.05 wt%) reduces red-scale formation (Fukagawa *et al.*, 1997).

Descalability is determined not only by the thickness of the scale but also the microstructure of the scale and that of the steel (Sheppard and Steen, 1970). The aim of this study is to identify particularly the behavior of silicon during the oxidation and the microstructure of the resulting scale. Also, the effects of alloying elements and temperature on scale formation need to be investigated.

Ⅱ Oxidation of Steel

2.1 Thermodynamic Aspects

The ultimate direction of an oxidation process can be predicted using the free energy. ΔG for the reaction:

$$x\mathrm{M} + \mathrm{O_2} = \mathrm{M_xO_2} \qquad (2.1.1)$$

where $\mathrm{M_xO_2}$ is the product of metal M and oxygen $\mathrm{O_2}$. Then,

$$\Delta G = \Delta G^0 + RT\ln K \qquad (2.1.2)$$

where ΔG^0 is the standard Gibbs free energy, T is temperature, R is the gas constant ($= 8.31$ J K^{-1} mol^{-1}) and the equilibrium constant, K, can be written as,

$$K = \frac{\left(a_{M_xO_2}\right)}{(a_M)^x \cdot \left(P_{O_2}\right)} \qquad (2.1.3)$$

Here a_{MO_2}, a_M are the activities of metal oxide and metal, and P_{O_2} is the partial pressure of oxygen. In most cases, a_{MO_2} is assumed to be 1. The reaction is spontaneous only if ΔG is negative and in equilibrium (i.e. $\Delta G = 0$), the equation (2.1.2) becomes as

$$\Delta G^0 = -RT \ln K \qquad (2.1.4)$$

Equations (2.1.3) and (2.1.4) determine the minimum oxygen partial pressure to form the metal oxide. The oxide can be produced if the pressure of oxygen is higher than calculated.

In order to predict whether the reaction occurs under given conditions, the Ellingham diagram, which is a plot of the standard free energy of formation of

selected oxides as a function of temperature, Fig. 2.1.1, can be used (Birks *et al.*, 2006). For pure iron, there are three different oxides: wüstite (FeO), magnetite (Fe_3O_4), and hematite (Fe_2O_3) as shown in the Fe-O diagram in Fig. 2.1.2. The scale is formed in increasing order of oxygen content, going from substrate to gas. At high temperatures, it is reported that the average thickness ratio of scale layers are found as wüstite: magnetite: hematite = 95:4:1 (Paidassi, 1958; Chen and Yeun, 2003).

For the steel, the microstructure of the oxide scale is complex and depends on many factors such as chemical composition, gap formation between scale and steel and the time of oxidation.
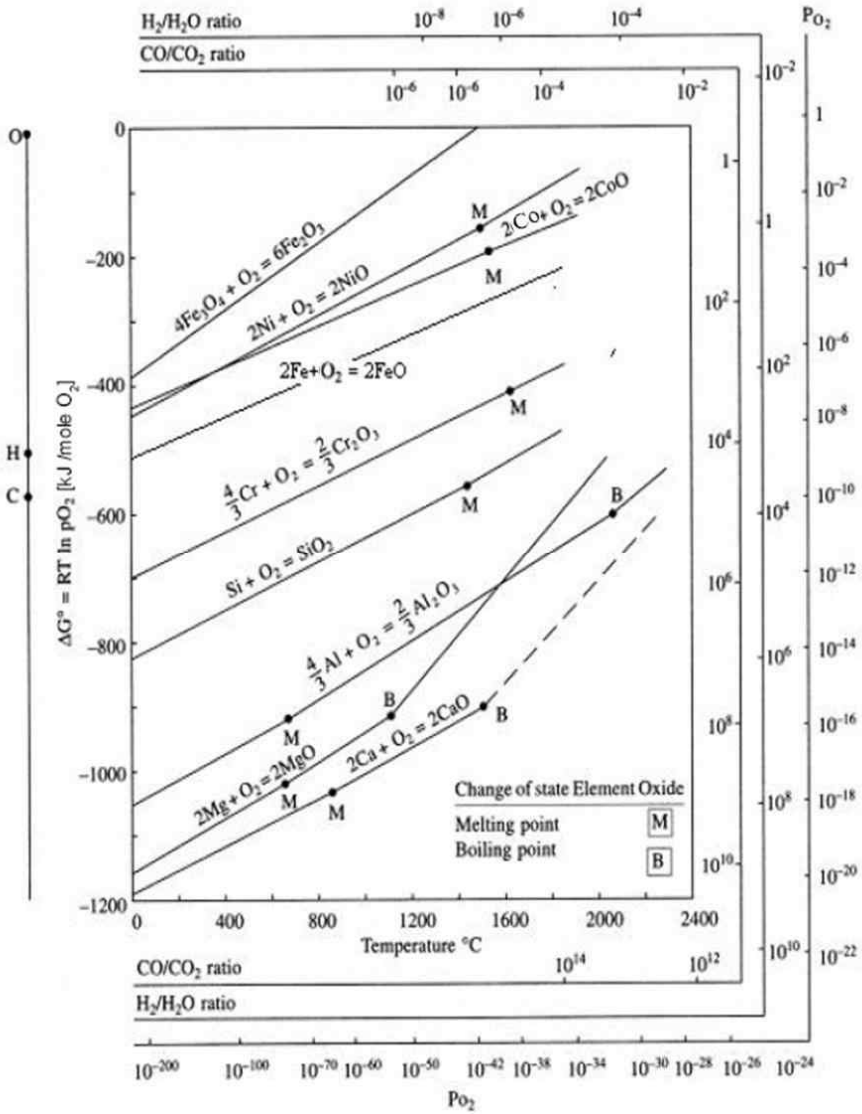
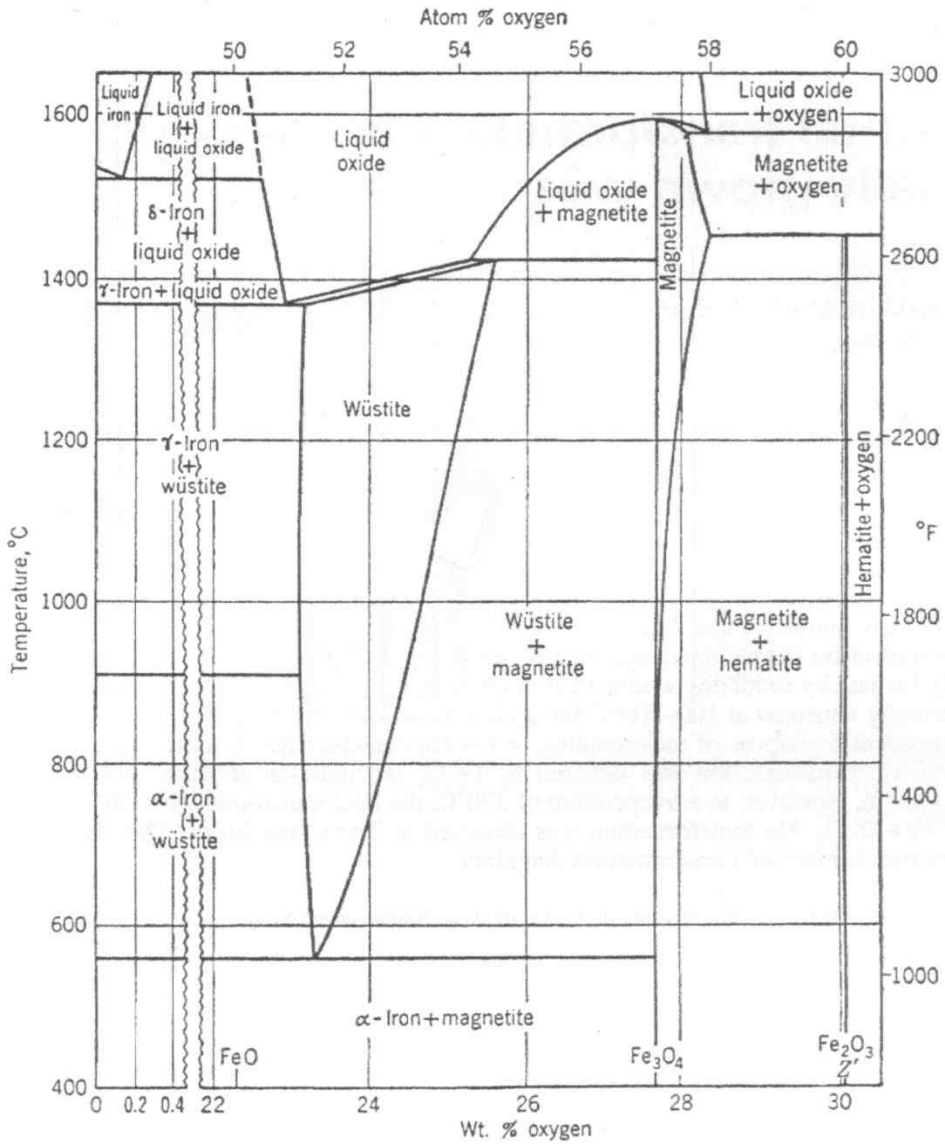Fig. 2.1.1 Ellingham Diagram (Birks *et al.*, 2006)

Fig. 2.1.2 The Fe-O phase diagram (Gleeson *et al.*, 2000)

2.2 Compounds of Iron Oxide

Wüstite has a face-centered cubic structure. The wüstite phase, FeO, is a p-type metal semiconductor that can exist over a wide range of stoichiometry. With its high cation vacancy concentration, the mobility of cations and electrons (via vacancies and electron holes) is also high. Its composition varies between its Fe and Fe_3O_4 boundaries (Toft, 1981). The cubic lattice constants for wüstite at the Fe and Fe_3O_4 boundaries at room temperature are 4.3108 and 4.2774 Å, respectively (Wyckoff, 1960). Wüstite only exists at temperatures above 570 °C. On cooling from temperatures above 570 °C, the wüstite layer will, in theory, undergo a eutectoid reaction. Even at lower temperatures the wüstite may undergo the eutectoid reaction forming a mixture of magnetite and iron (Chen and Yuen, 2001);

$$4FeO = Fe_3O_4 + Fe \qquad (2.2.1)$$

However, if the cooling rate is sufficiently rapid, the wüstite layer may be retained to a temperature range well below 570 °C before the onset of the eutectoid reaction. The unstable wüstite layer might gradually be oxidized to magnetite during the continuous cooling process at temperature below 570 °C, the overall reaction is

$$3FeO + O_2 = Fe_3O_4 \qquad (2.2.2)$$

The phase magnetite, Fe_3O_4, is an inverse spinel structure, which has divalent ions, Fe^{2+}, occupying octahedral sites and half of the trivalent ions, Fe^{3+},

occupying tetrahedral sites (Birks *et al.*, 2006). Defects occur on both sites and consequently iron ions may diffuse over both tetrahedral and octahedral sites. The composition of magnetite is known to correspond closely to its stoichiometry, Fe_3O_4. The cubic unit cell has a lattice constant of 8.396 Å at 25 °C (Abuluwefa *et al.*, 1996). Magnetite can be a non-stoichiometric compound which exhibits a cation deficiency: the iron to oxygen ratio lies in the range 0.750 to 0.744 (Harkins, 1984), however, this ratio is dependent upon both the oxygen pressure and the temperature.

There are two forms of hematite; the α and γ. The α-form has a trigonal structure with the ferric ions occupying octahedral sites. While the γ-form has a structure similar to magnetite, being a cation-deficient inverse spinel with an iron to oxygen ratio in the range 0.67 to 0.72. However, γ-Fe_2O_3 forms α-Fe_2O_3 above 400 °C and only this structure needs to be considered here. α-Fe_2O_3, has the trigonal structure with *a* and *c* for the hexagonal unit cell of hematite being; 5,035 and 13.72 Å, respectively at room temperature (Wyckoff, 1960).

2.3 Kinetics of Oxidation

The rate of oxide growth can differ as shown in Fig. 2.3.1. The general law can be written as

$$z^n = kt + C \qquad (2.3.1)$$

where z is the thickness of the oxide, k is rate constant, t is the oxidation

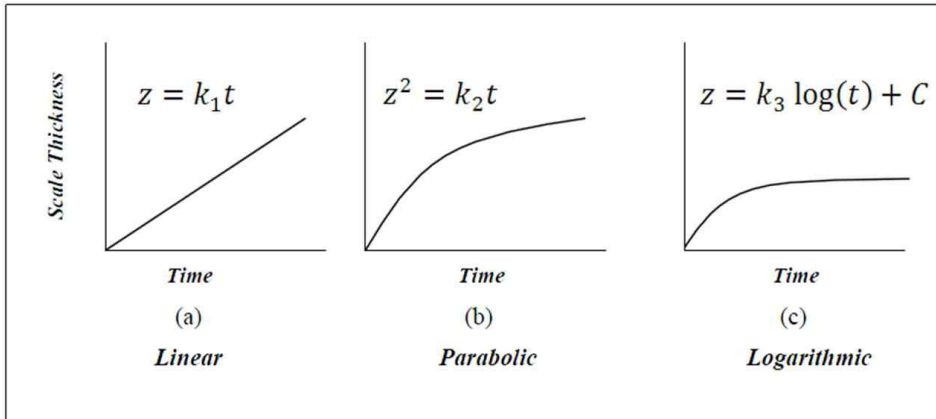time, C is the integration constant, and n is the power exponent.

Fig. 2.3.1 Schematic illustration of the change in scale thickness with time

for the various types of oxidation (Stott, 1987)

When n equals 1, the reaction is said to obey the linear rate law. In the absorption and nucleation process, the rate-controlling step is the steel surface or the phase boundary interface reaction as described by (2.3.2) and oxidation obeys a linear rate law.

$$Fe = Fe^{2+} + 2e^- \text{ (steel/oxide)}$$

$$O_2 + 2e^- = O^{2-} \text{ (oxide/gas)} \qquad (2.3.2)$$
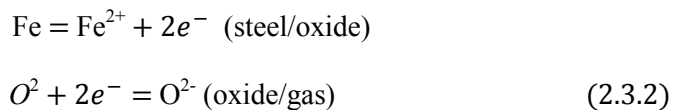
For example, initially after exposure of the steel, the oxygen mass transfer to the outer scale surface controls the rate of scale growth since Fe^{2+} transfer is relatively efficient at the small-thickness scale. In such a case, the thickness of the scale formed is directly proportional to time and independent of the scale

thickness (Sachs and Tuck, 1968).

When n equals 2, the reaction is said to obey the parabolic rate law. In the high temperature growth, the oxidation rate is controlled by diffusion through the scale (Rapp, 1984, Chang and Wei, 1989) and the classic Wagner theory predicts parabolic kinetics. The following are the assumptions made in Wagner`s theory.

1. The formed oxide scale is dense, well adhered to a metal surface and non-porous.

2. Oxygen has only limited solubility in the metal.

3. There are no space charge effects across the oxide and at the metal/oxide and oxide/gas interface.

4. At each place in the scale as well as at the interfaces, local thermodynamic equilibrium is established.

This type of reaction prevails if the diffusion process of reactants through the scale is determined by

$$\frac{dz}{dt} = \frac{k}{z} \qquad (2.3.3)$$

where z is the scale thickness, t is time and k is the rate constant. Then,

$$z^2 = 2k\mathrm{t} \qquad (2.3.4)$$

In addition, the logarithmic rate laws represent the low temperature (< 200 ºC) oxidation processes (Chang and Wei, 1989; Birks *et al.*, 2006). In this case, the rate determining process is transportation of ions due to electric fields in the

oxide film.

In practice, the oxidation reactions follow a combination of rate laws. For example, at high temperatures reactions may be interface controlled (linear) during initial stages and diffusion limited (parabolic) after extended oxidation.

2.4 Effects of Alloying Elements

The oxide scale of steel is complicated by the effects of alloying elements. It is not easy on the basis of literature to determine precisely which effects are due to a single addition of the element on the oxidation kinetics and the microstructure of scale.

In general, the main effect of alloying elements less noble than iron, such as Al and Si, on the oxidation is the formation of a protective layer, enriched in alloying elements at the scale/steel interface. On the other hand, those elements more noble than iron, such as nickel and copper are rejected at the scale/steel interface, and act to form a tight mechanical bond, thereby increasing the oxidation resistance (Chang and Wei, 1989; Birks *et al.*, 2006).

2.4.1 Silicon

Addition of Si to iron reduces the oxidation rate and the scale thickness decreases with an increase in the Si content. This is explained by the formation of a silicon-

rich layer at the scale/steel interface due to its less noble behaviour than iron. The SiO_2-rich inner scale layer formed with alloys containing 2 to 3 wt% Si or more results in a reduced oxidation rate. In low-alloy steel, the SiO_2 formed at the scale/steel interface reacts with FeO to form the spinel Fe_2SiO_4. The accumulated Fe_2SiO_4 at the interface slows the diffusion of iron from the substrate to the scale, since the diffusion of iron through it is much slower than through FeO (Darken and Gurry, 1945; Tuck, 1965; Taniguchi *et al.*, 2001).

The Fe_2SiO_4 has a melting temperature about 1173 ºC so melting may happen during the hot rolling process. When Fe_2SiO_4 melts, it penetrates into FeO and as it cools, it can act as a "glue" to bind FeO to the steel surface (Fukagawa *et al.*, 1994; Taniguchi *et al.*, 2001). It is found that the resultant Fe_2SiO_4 yields scale that is not completely removed by high pressure hydraulic descaling (Fukagawa *et al.*, 1994; Okada *et al.*, 1995; Chen and Yuen, 2001) and is difficult to remove by pickling (Chattopadhyay and Chanda, 2008).

2.4.2 Aluminum

Similar to Si, Al forms an enriched layer at the scale/steel interface and retards iron diffusion thus reducing the oxidation rate. The exact nature of such aluminum-rich layers appears to vary with the Al content of the steel, the temperature and the oxidizing atmosphere. For example, if iron with 1 wt% Al is oxidized in 1 atm O_2 at 500 to 700 ºC, then the aluminum-rich layer is Al_2O_3. If it is done in the same atmosphere but at 700-900 ºC, then the layer is $FeAl_2O_4$

spinel (Saegusa and Lee, 1966).

Moreover, the temperature of FeO formation increases in the Al-added steel. For example, in the steel with 1.8 wt% Al it is 798 ºC, which is higher than 570 ºC from the Fe-O phase diagram. Since the diffusion of iron in magnetite is slower than that in FeO, it contributes to the slow oxidation rate (Huang and Zhu, 1983).

2.4.3 Nickel

Thermodynamically, Ni is not easily oxidized and FeO contains a small concentration of Ni as seen in Fig. 2.1.1. The maximum solubility of nickel in FeO is reported to be 0.12 wt% at 700 ºC increasing to 2.0 wt% at 1100 ºC (Viktorovich *et al.*, 1966; Viktorovich and Lisovskii, 1966) . On the other hand, the maximum nickel concentration in the steel phases is 65 wt% at 700 ºC increasing to 84.7 wt% at 1100 ºC (Viktorovich and Lisovskii, 1966). The iron in nickel-added steel is selectively oxidized and Ni is accumulated at the scale/steel interface. Since the diffusion coefficient of nickel in iron is small, it cannot diffuse rapidly back into the core and hence its concentration becomes much higher at the interface than in the core (Brown and Wold, 1969). For example, nickel enrichment in the Fe with 1 wt% Ni surface oxidized in oxygen at 1000 ºC almost approached 70 wt% (Wulf *et al.*, 1969). This selective oxidation of iron produces a rough scale/steel interface and entanglement of nickel in the scale (Morris and Smeltzer, 1967; Wulf *et al.*, 1969).

15

Ⅲ Red-scale

3.1 Mechanism of Red-scale Formation

A thick layer of oxide scale forms during the reheating process. The hydraulic descaler near the exit of the reheat furnace removes it, however, after the descaling process there might be remnants of FeO. If the FeO is fractured by hot rolling, the underlying region is exposed to air and hence to an excess of oxygen together with iron ions from the substrate. Then the reaction, $FeO \rightarrow Fe_3O_4 \rightarrow Fe_2O_3$ is accelerated and the final product, powdered-Fe_2O_3 is the red-scale as mentioned before. Therefore, the residual scale before rolling is the cause of red scale formation (Fukagawa *et al*., 1994). The process is illustrated schematically in Fig. 3.1.1.
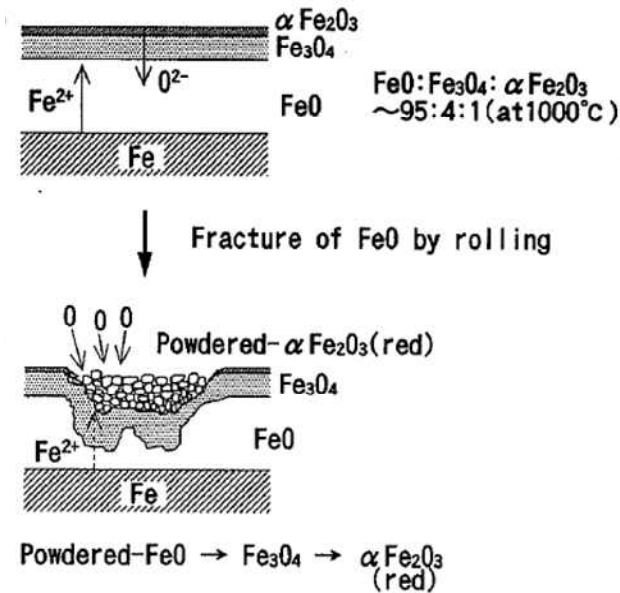
Fig. 3.1.1 Mechanism of red-scale formation by fracture of FeO layer

(Fukagawa *et al*., 1994)

3.2 Red-scale in Si-added Steel

When silicon is added, Fe_2SiO_4 is formed at the scale/steel interface. As shown in the FeO-SiO_2 phase diagram in Fig. 3.2.1, the Fe_2SiO_4 starts to melt at a temperature of about 1173 ºC during the reheating process. When this happens, the liquid phase penetrates into grain boundaries of the FeO (Palin, 1965); the higher the silicon content, the deeper is the penetration (Taniguchi *et al*., 2001). As it cools, the eutectic compound FeO/Fe_2SiO_4 forms with a morphology that anchors the oxide after solidification.

It is reported that the grain boundary eutectic compound makes it difficult to descale the steel because of the anchoring effect, by which the scale is firmly connected to the steel substrate (Okita *et al*., 1989). Furthermore, the depth of invasion of the FeO/Fe_2SiO_4 eutectic compound into the FeO grain boundaries greatly deteriorates the ability to descale (Tuck and Barlow, 1972).
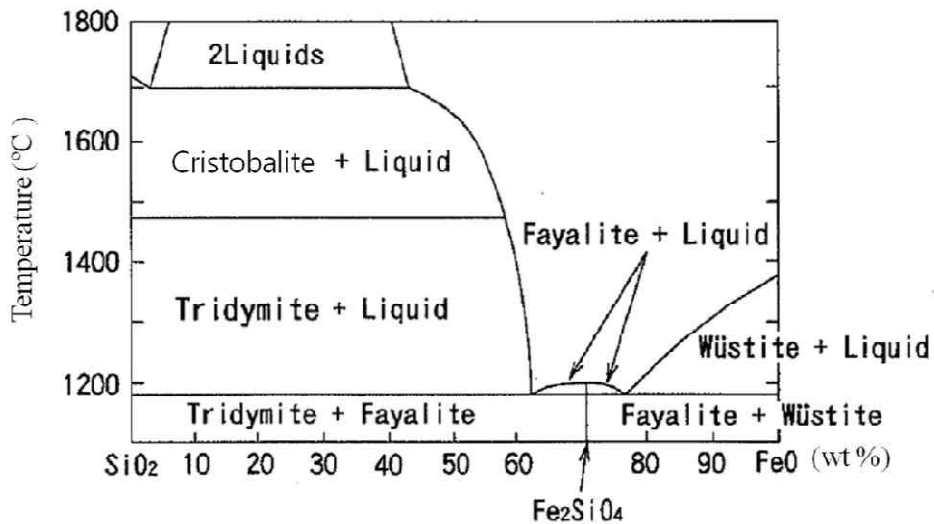
Fig. 3.2.1 $FeO-SiO_2$ phase diagram (Levin *et al.*, 1964)

In addition, the hardness of the FeO/Fe_2SiO_4 eutectic compound at high temperature is much greater than that of FeO (Amano *et al.*, 2006), as seen in Table 3.2.1. This can also explain the poor descaling ability result of the eutectic compound.

	Hardness (GPa)		
Oxides	Fe	Fe-1.5 wt% Si	Fe-3.0 wt% Si
Fe_2O_3	-	0.32	0.53
Fe_3O_4	0.08	-	-
$FeO+Fe_3O4$	0.05	-	-
FeO	0.05	-	-
Fe_2SiO_4+FeO	-	0.50	-
Fe_2SiO_4	-	-	0.63
Substrate	0.12	0.04	0.03

Table 3.2.1 High temperature hardness of oxide scales on Fe- (0, 1.5, 3.0) wt% Si alloys and its substrates at 1000 ºC after oxidation at 1000 ºC for 18 ks (Amano *et al.*, 2006)

Fukagawa *et al*. found the same results by reproducing the scale by laboratory hot rolling. The slabs were heated at 1220 ºC for 2 h in an atmosphere of 77.1% N_2 + 14.3% H_2O + 8.2% CO_2 so primary scale was formed and then it was removed using a hydraulic descaler. For the steel with 0.54 wt% Si, remaining FeO was found after descaling. On the other hand, a clean interface was found for the steel with only 0.005 wt% Si. Fig. 3.2.2 illustrates the mechanism of red-scale formation in Si-added steel (Fukagawa *et al*., 1994).
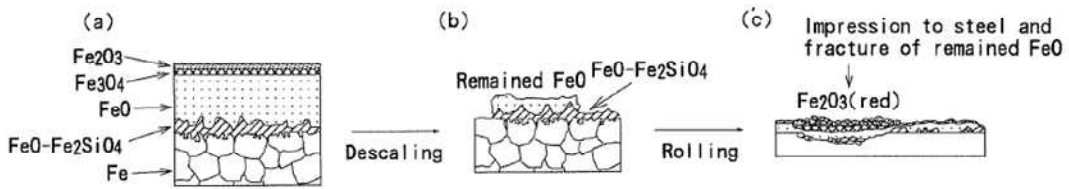
Fig. 3.2.2 Mechanism of red-scale formation in Si-added hot rolled steel

(Fukagawa *et al*., 1994)

(a) Formation of the primary scale;

(b) Remainder of the scale after descaling;

(c) Red-scale formation.

3.3 Effects of Other Elements on Red-scale

3.3.1 Nickel

It is found that the removal of nickel reduces red-scale by improving the ability to descale (Fukagawa *et al*., 1996, Asai *et al*., 1997). Since Ni is more noble than iron, the iron in nickel-added steel is selectively oxidized and the concentration of Ni is enriched at the interface. The grain boundaries then oxidize preferentially, internal oxides precipitate and Ni enriches around them. Heterogeneously enriched Ni makes the oxidation irregular and results in the rough scale/steel interface (Fukagawa *et al*., 1996). The mechanism of the rough interface formation is explained in Fig. 3.3.1.
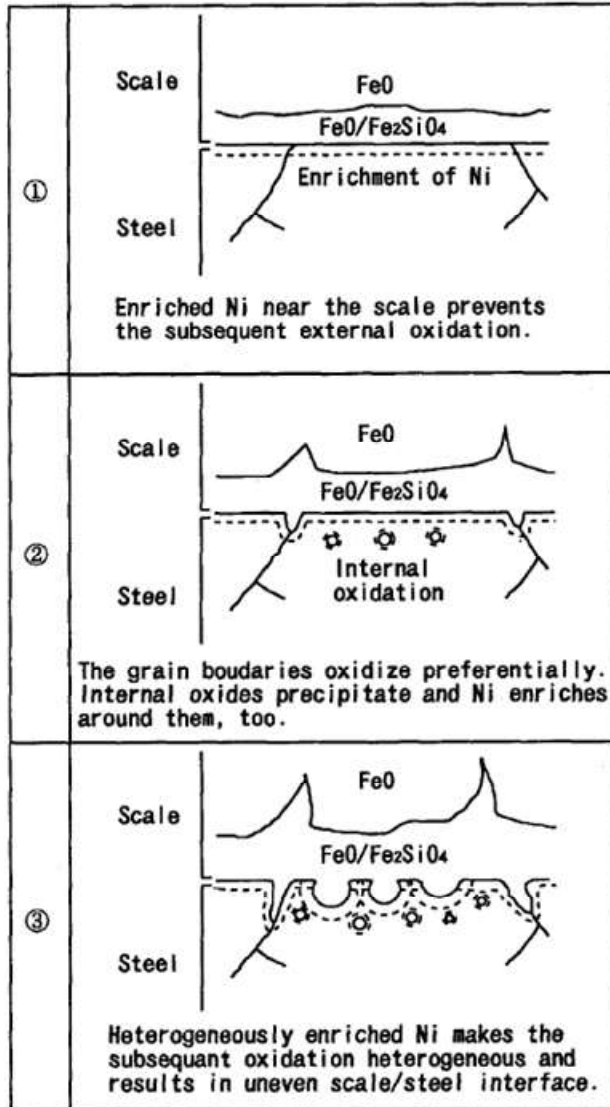
Fig. 3.3.1 Mechanism of irregular morphology formation in the interface between primary scale and steel (Fukagawa *et al*., 1996)

The interface roughness increases with Ni addition and it leads to poor descalibility. This agrees with another result of Asai *et al*. Fig. 3.3.2 shows the

scale/steel interfaces of 0.1 wt% Si steel with different concentrations of Ni. In the case of Ni content of 0.001 wt%, the interfaces were flat, but at 0.1 wt%, they became uneven at all oxidation temperatures. For the steel with 0.1 wt% Ni, the remaining scale after descaling was thicker than lower nickel alloy as shown in Fig. 3.3.3 (Asai *et al*., 1997).
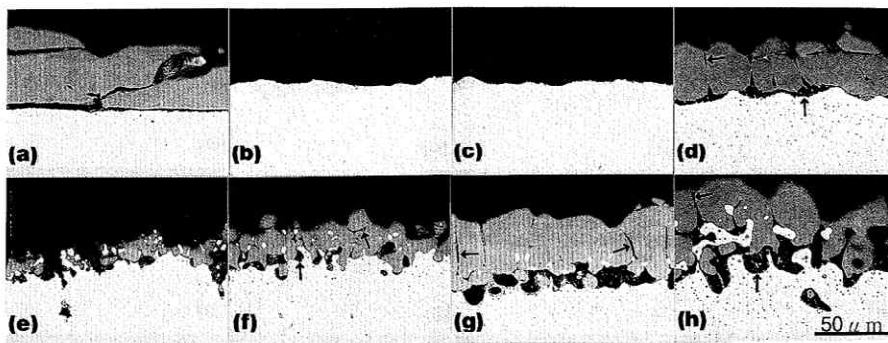
Fig. 3.3.2 Optical micrographs of the scale/steel interface in 0.1 wt% Si steels. Arrows in the figure indicates fayalite (Asai *et al*., 1997):

Steel with 0.001 wt% Ni oxidized for 60 min in air at

 (a) 1100 ℃, (b) 1150 ℃, (c) and (d) 1250 ℃;

steel with 0.1 wt% Ni oxidized in air for 60 min at

 (e) 1100 ℃, (f) 1150 ℃, (g) 1200 ℃ and (h) 1250 ℃.
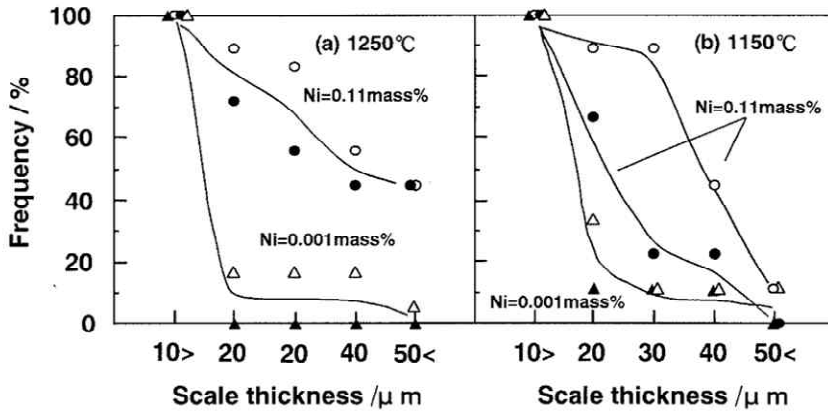
Fig. 3.3.3 Thickness distributions of the residual scale after hydraulic descaling in 0.1 wt% Si steels with nozzle height of 600 mm (open marks) and 300 mm (solid marks), heated in air for 60 min at (a) 1200 ºC and (b) 1100 ºC (Asai *et al.*, 1997)

3.3.2 Phosphorus

For both 0.5 wt% Si steel and 1.5 wt% Si steel oxidized at 1260 ºC, the fraction of red-scale area was decreased by adding P up to 0.1 wt% as shown in Fig. 3.3.4 (Fukagawa *et al.*, 1997). It is found that P forms P_2O_5 during oxidation and it lowers the eutectic temperature of FeO and Fe_2SiO_4, Figs. 3.3.5 and 3.3.6. Thus, solidification is suppressed and the presence of the liquid compound at the scale/steel interface contributes to the descaling ability.
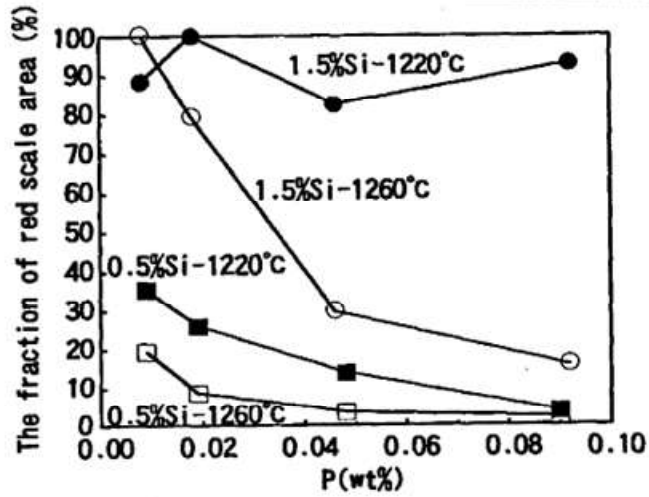
Fig. 3.3.4 Effect of Si, P and slab-reheating (oxidation) temperature on the

fraction of red-sale area after reproduction tests (Fukagawa *et al*., 1997)
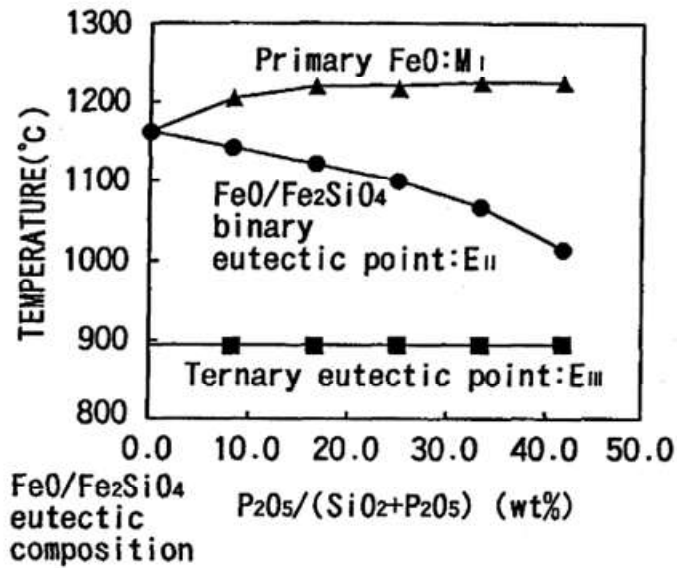

Fig. 3.3.5 Effect of P_2O_5 content on the FeO/Fe$_2$SiO$_4$ binary eutectic point
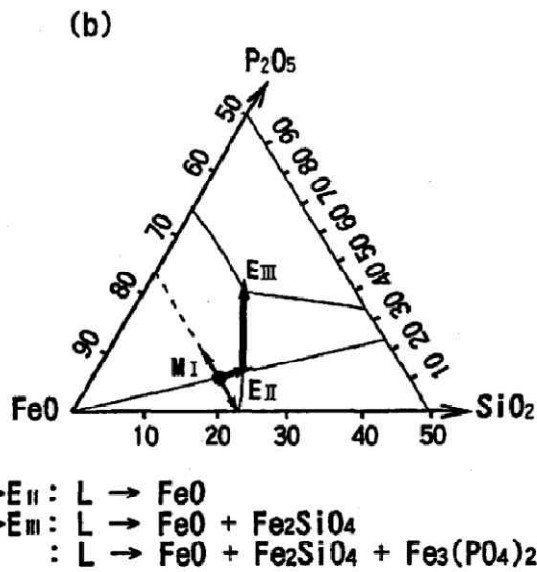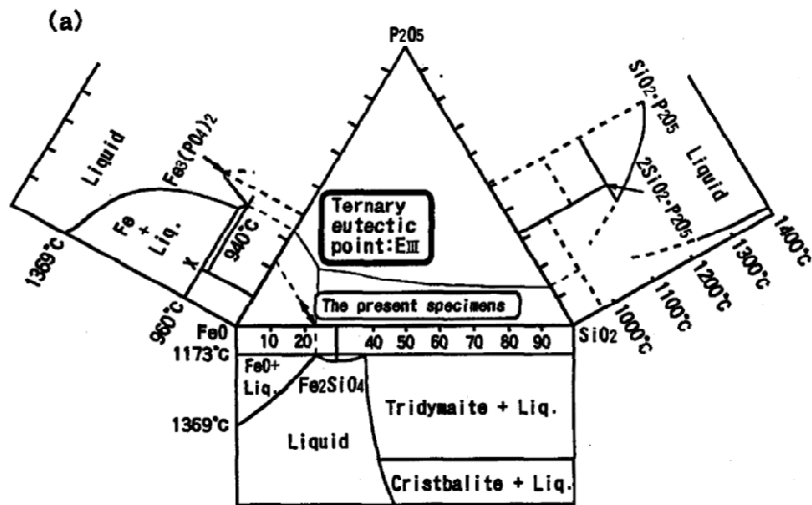
(Fukagawa *et al*., 1997)

(a)

(b)

$M_I \rightarrow E_{II}$: $L \rightarrow FeO$
$E_{II} \rightarrow E_{III}$: $L \rightarrow FeO + Fe_2SiO_4$
E_{II} : $L \rightarrow FeO + Fe_2SiO_4 + Fe_3(PO_4)_2$

Fig. 3.3.6 FeO-SiO$_2$-P$_2$O$_5$ ternary eutectic system with concentration unit, wt%

(Fukagawa *et al*., 1997)

Ⅳ Experimental

4.1 Alloys

Four different alloys were fabricated and used in order to investigate the effects of Si, Ni and Al on the oxidation. The alloys were produced by POSCO. The manufacturing steps consisted of vacuum melting and casting to produce a 30 kg ingot for each alloy. It was then hot-rolled into a 20 mm plate. The compositions are shown in Table 3.1. Alloy 1 and Si Alloy are designed to find the effect of silicon on the oxidation. Ni Alloy is for the effect of nickel, and Al Alloy is made to investigate the effect of aluminum on the formation of red-scale.

Steel	C	Si	Mn	Ni	Al	Fe
Alloy 1	0.1	-	1.5	-	-	balance
Si Alloy	0.1	0.943	1.54	-	-	balance
Ni Alloy	0.1	1.0	1.50	0.197	-	balance
Al Alloy	0.101	1.01	1.49	-	0.216	balance

Table 4.1.1 The compositions of the alloys in wt%

4.2 Oxidation Test

Samples were cut into $10 \times 7 \times 5$ mm using standard techniques and the largest surfaces were ground using silica carbide paper to the final of 2000 grit. Following this, they were ultrasonically treated in ethanol and oxidized in a furnace. The oxidation test was carried out in the alumina tube furnace, at 1000 °C and 1250 °C in air. The sample was cooled to room temperature after 2 h. The cooling rate was kept slow in order to reduce the thermal shock.

4.3 Microscopy

Oxidized sample was observed using optical microscopy (OM), scanning electron microscope (SEM), electron microprobe analysis (EPMA) and transmission electron microscopy (TEM). The sample for the OM and SEM was mounted and its cross section was investigated. It was ground to the 2000 grit, followed by polishing using 3, 1 and 0.25 μm diamond paste. Since the oxide is brittle and has many pores, care is needed during grounding and polishing. Prior to the microscopy analysis, it was coated with gold in order to increase the conductivity. OM instrument was Olympus BX60M and SEM instruments were JEOL JSM 5900 and CARL Zeiss ULTRA 55 FE-SEM.

For TEM, the sample was prepared by focused ion beam (FIB) from its cross section. It was examined in a PHLIPS CM200 transmission electron microscope operated at 200 kV.

The composition and element distribution were analyzed by the energy dispersive

X-ray spectra (EDS) and wavelength dispersive spectroscopy (WDS).

4.4 X-ray Diffraction Analysis

Samples after oxidation test were powered and analyzed by BRUKER D8 X-ray diffractometer (XRD). Beams were step scanned at speed of 0.2º per minute using Cu K_α X-rays.

Ⅴ Results

5.1 Prediction of Oxides Formation

To predict the oxide formation, the free energies of the oxide per one mole of O_2 was calculated with a regarding of the actual composition of the steel and partial pressure of oxygen. In this study, oxides formation at 1000 ℃ and 1250 ℃ with Fe - 0.1C - (0 ~ 13) Si wt% steel was investigated.

First, the equilibrium phase fraction of steel depending on the silicon concentration was investigated with the base alloy Fe-0.1 C wt% steel with TCFE database by ThermoCalc. The results are shown in Fig. 5.1.1. At 1000 ℃ the equilibrium phase is fully FCC austenite with the silicon containing steel up to 2 wt% and it is fully BCC ferrite with the silicon containing steel more than 8 wt%. For Fe - 0.1C - (2 ~ 8)Si wt% steel, a combination of BCC ferrite and FCC austenite was the equilibrium state for a given temperature; however, oxides were assumed to form on BCC ferrite because the diffusion in BCC ferrite is faster than diffusion in FCC austenite as in Fig. 5.1.2.
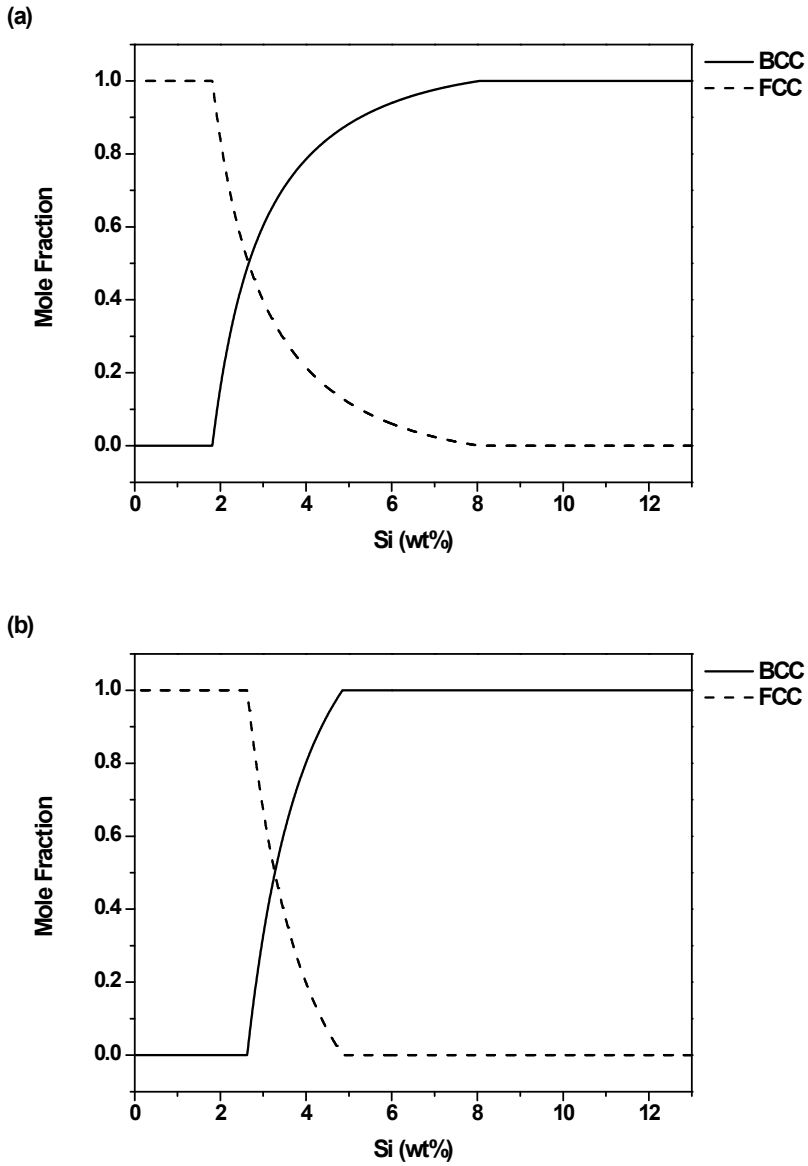
Fig. 5.1.1 Equilibrium mole fractions of BCC ferrite and FCC austenite in Fe – 0.1 C – (0 ~ 13) Si wt% steel at (a) 1000 ℃ and (b) 1250 ℃. Solid lines indicate BCC ferrite and dashed lines indicate FCC austenite.
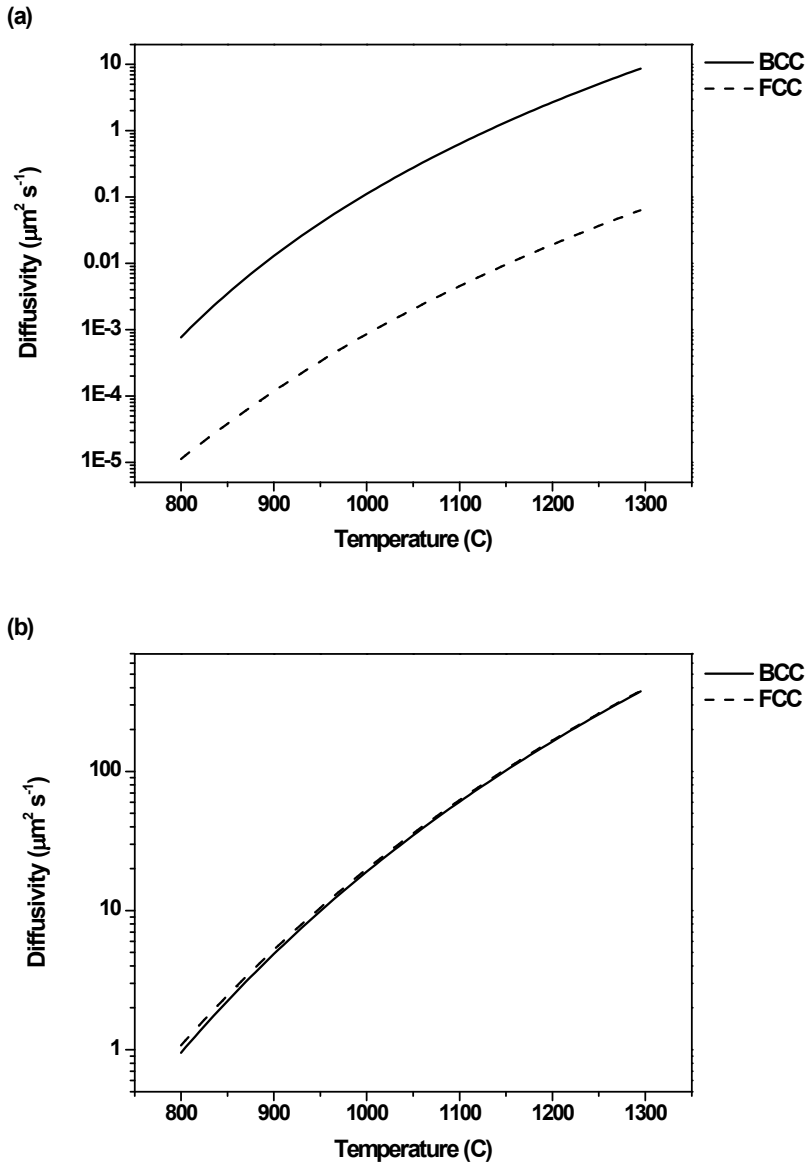
(a)

(b)

Fig. 5.1.2 Diffusivity of silicon and oxygen in BCC ferrite and FCC austenite obtained from MOBFE1 database with DICTRA. (a) indicates diffusivity of silicon and (b) indicates diffusivity of oxygen.
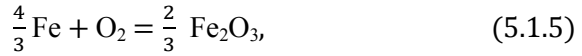
For oxides formation, ΔG for the reaction:

$$2Fe + O_2 = 2\,FeO, \tag{5.1.1}$$

$$\Delta G_{2FeO} = \Delta G^o_{2FeO} + RT\ln\frac{(a_{FeO})^2}{(a_{Fe})^2(P_{O_2})} \tag{5.1.2}$$

$$\frac{3}{2}\,Fe + O_2 = \frac{1}{2}\,Fe_3O_4, \tag{5.1.3}$$

$$\Delta G_{\frac{1}{2}Fe_3O_4} = \Delta G^o_{\frac{1}{2}Fe_3O_4} + RT\ln\frac{(a_{Fe_3O_4})^{\frac{1}{2}}}{(a_{Fe})^{\frac{3}{2}}(P_{O_2})} \tag{5.1.4}$$

$$\frac{4}{3}\,Fe + O_2 = \frac{2}{3}\,Fe_2O_3, \tag{5.1.5}$$

$$\Delta G_{\frac{2}{3}Fe_2O_3} = \Delta G^o_{\frac{2}{3}Fe_2O_3} + RT\ln\frac{(a_{FeO})^{\frac{2}{3}}}{(a_{Fe})^{\frac{4}{3}}(P_{O_2})} \tag{5.1.6}$$

$$Si + O_2 = \,SiO_2, \tag{5.1.7}$$

$$\Delta G_{SiO_2} = \Delta G^o_{SiO_2} + RT\ln\frac{a_{SiO_2}}{a_{Si}(P_{O_2})} \tag{5.1.8}$$

$$Fe + \frac{1}{2}\,Si + O_2 = \frac{1}{2}\,Fe_2SiO_4, \tag{5.1.9}$$

$$\Delta G_{\frac{1}{2}Fe_2SiO_4} = \Delta G^o_{\frac{1}{2}Fe_2SiO_4} + RT\ln\frac{\sqrt{a_{Fe_2SiO_4}}}{(a_{Fe})(P_{O_2})\sqrt{a_{Si}}} \tag{5.1.10}$$

In this calculation, the activities of FeO, Fe_3O_4, Fe_2O_3, SiO_2 and Fe_2SiO_4, were assumed to be 1 because those phases were considered to be pure solids, which are the reference states. Also, the reference states for Fe, Si and O_2 were considered to be BCC ferrite, diamond silicon, gas oxygen, respectively. Fig. 5.1.3 shows the activities of silicon and iron in Fe – 0.1 C – (0 ~ 13) Si wt% steel. The reference states of Si and Fe are diamond and BCC, respectively.

The formation energy was obtained from the literature (Lee, 1999) and SUB_SGTE database by using MTDATA software. Since the pressure of oxygen is same for the all the reaction, ΔG of oxides for one mole of O_2 were calculated. Fig. 5.1.3 shows the formation energies of oxides in Fe – 0.1 C – (0 ~ 13) Si wt% steel oxidized at 1000 ºC and 1250 ºC with $P_{O_2} = 0.2$ atm. In air, formation energies of Fe_2O_3, Fe_3O_4, FeO, Fe_2SiO_4 and SiO_2 were negative, thus those oxides could form spontaneously. As increasing the silicon concentration in steel, the driving force for forming Fe_2O_3, Fe_3O_4 and FeO decreased but driving force for Fe_2SiO_4 and SiO_2 increased. It was noted that the driving force for forming SiO_2 was larger than that of Fe_2SiO_4 or FeO independent of the silicon concentration.
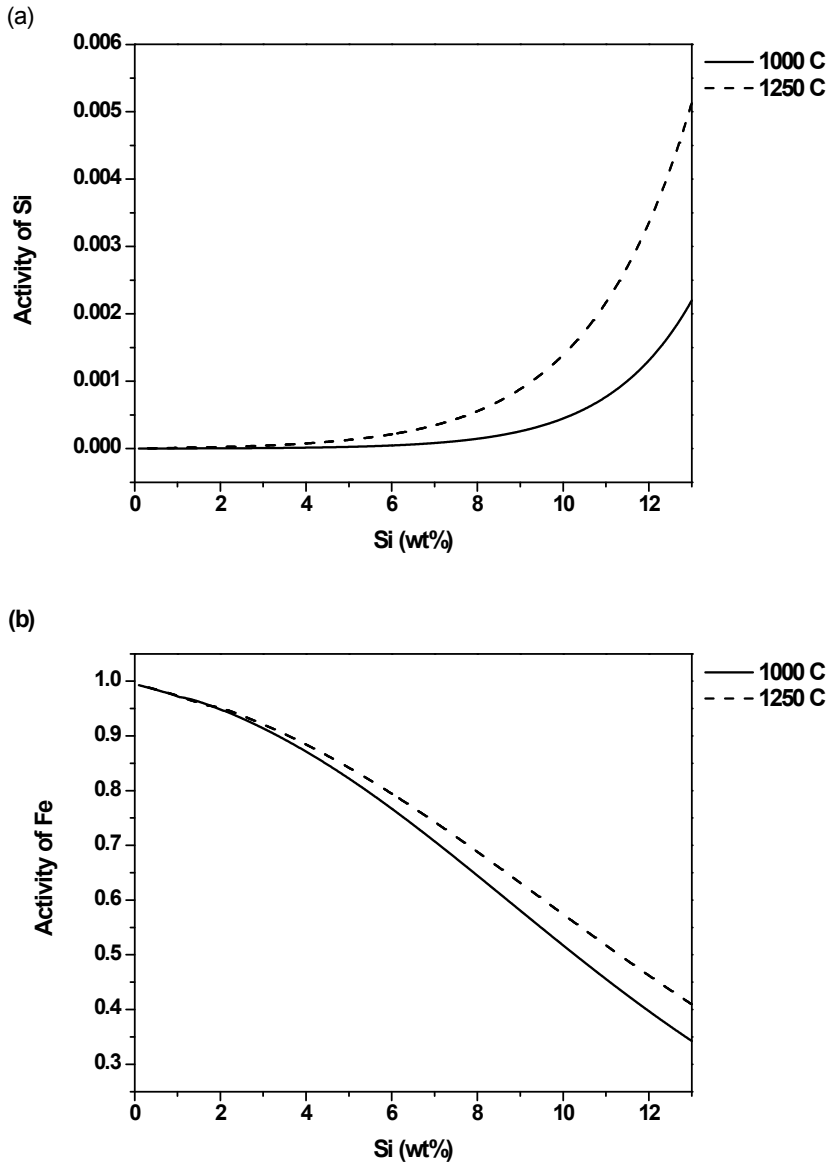
Fig. 5.1.3 The activities of (a) silicon and (b) iron in Fe – 0.1 C – (0 ~ 13) Si wt% steel. The reference states of Si, Fe are diamond phase and BCC ferrite, respectively. Solid lines, dashed lines show activities at 1000 ℃ and 1250 ℃.
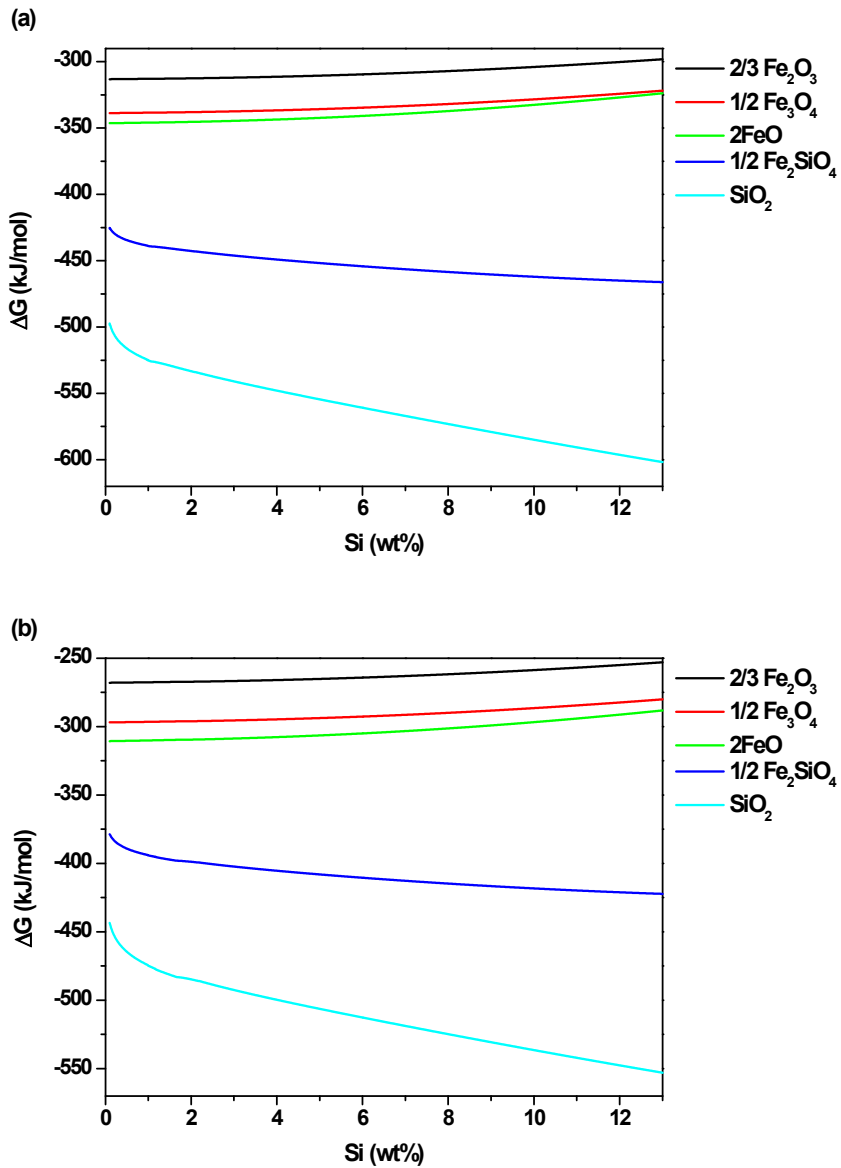
(a)

(b)

Fig. 5.1.4 Formation energies of oxides in Fe – 0.1 C – (0 ~ 13) Si wt% steel oxidized in air at (a) 1000 ºC and (b) 1250 ºC. Black, red, green, navy, blue lines show formation energies of 2/3 mole of hematite, 1/2 mole of magnetite, 2 mole of wüstite, 1/2 mole of fayalite and 1 mole of tridymite, respectively.

Since oxidation involves the partial pressure of oxygen which varies depending on the time, the equilibrium phases of oxides formed at 1000 ºC and 1250 ºC of Fe – 0.1 C – 1 Si wt% steel and Fe – 0.1 C – 13 Si wt% steel depend on the oxygen pressure were calculated. The results are shown in Figs. 5.1.5 and 5.1.6. For 1250 ºC, the liquid Fe_2SiO_4 was considered instead of the solid phase because its melting temperature is below 1250 ºC. Since a high value of oxygen pressure is needed to form an oxide which driving force is small, these results are in good agreements with the results in Fig. 5.1.4.
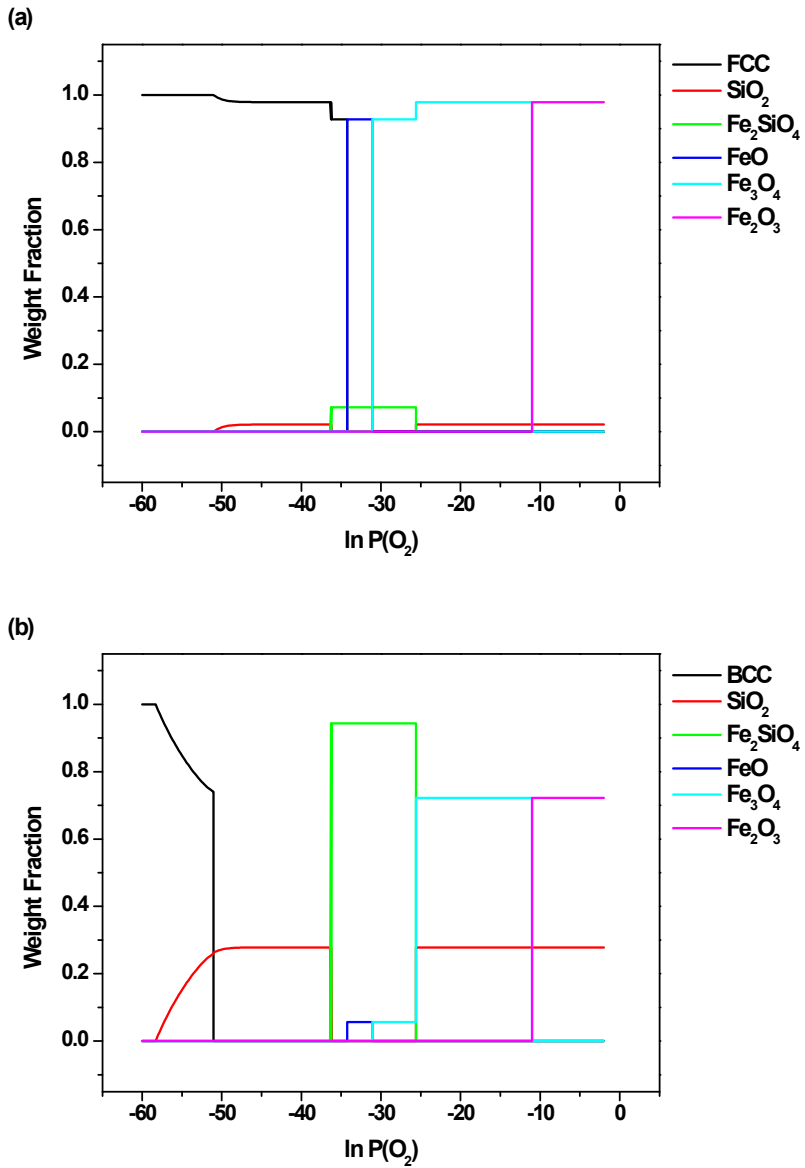
Fig. 5.1.5 Obtained equilibrium weight fractions of oxides formed at 1000 °C by using ThermoCalc. (a) indicates oxides on Fe – 0.1 C – 1 Si wt% steel and (b) indicates oxides on Fe – 0.1 C – 13 Si wt% steel.
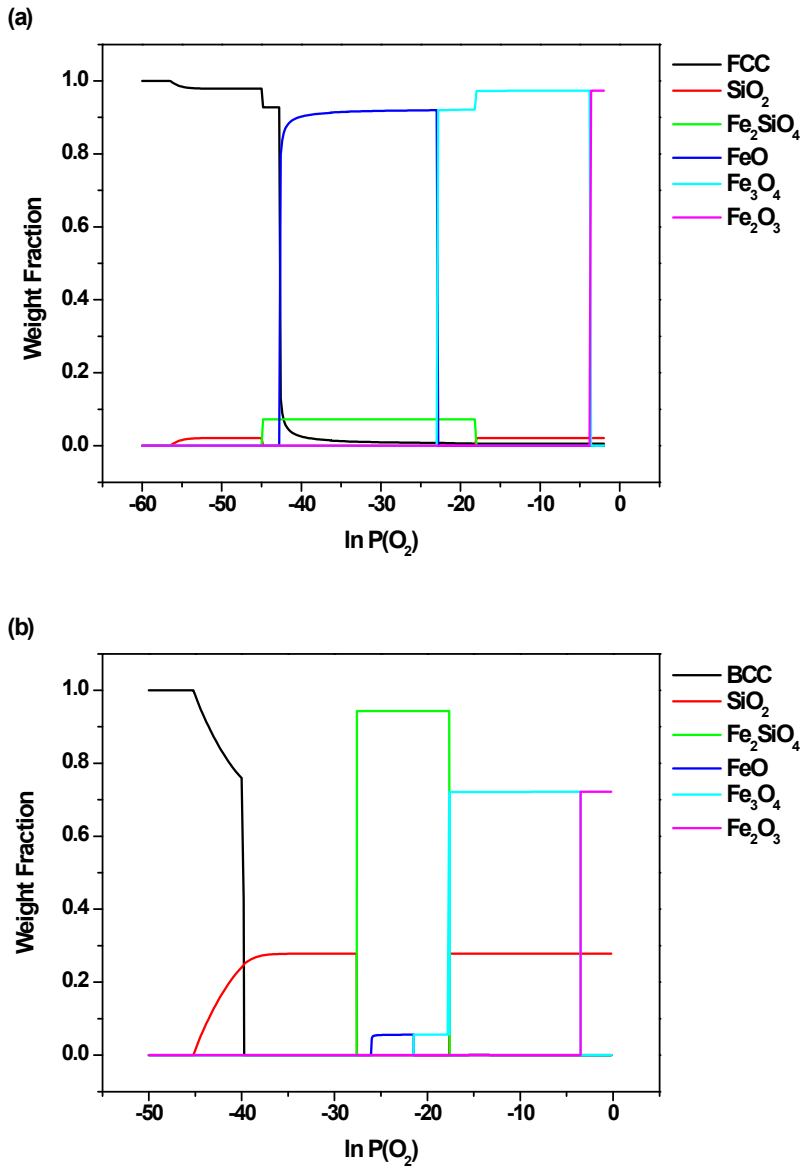
Fig. 5.1.6 Obtained equilibrium weight fractions of oxides formed at 1250 °C by using ThermoCalc. (a) indicates oxides on Fe – 0.1 C – 1 Si wt% steel and (b) indicates oxides on Fe – 0.1 C – 13 Si wt% steel.

However, it was noted that FeO, SiO_2 and Fe_2SiO_4 cannot exist in equilibrium at the single oxygen pressure for a given temperature. It can be explained thermodynamically by considering a reaction (5.1.11).

$$SiO_2 + 2Fe + O_2 = Fe_2SiO_4,\qquad(5.1.11)$$
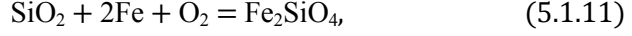
For this reaction, the Gibbs free energy ΔG_1 can be obtained as

$$\Delta G_1 = \Delta G_1{}^o + RT\ln\frac{\sqrt{a_{Fe_2SiO_4}}}{(a_{SiO_2})(a_{Fe})^2(P_{O_2})}\qquad(5.1.12)$$

Here,

$$\Delta G_1{}^o = 2\Delta G^o_{\frac{1}{2}Fe_2SiO_4} + \Delta G^o_{SiO_2}\qquad(5.1.13)$$

Also, a_{SiO_2} and $a_{Fe_2SiO_4}$ were assumed to be 1.

In order to form FeO, equation (5.1.14) should be satisfied from equation (5.1.2).

$$(a_{Fe})^2(P_{O_2}) > \exp\left(\frac{\Delta G^o_{2FeO}}{RT}\right)\qquad(5.1.14)$$

Then equation (5.1.12) becomes

$$\Delta G_1 < \Delta G_1{}^o - \Delta G^o_{2FeO}\qquad(5.1.15)$$

From the literature (Lee, 1999) and SUB_SGTE database,

$$\Delta G^o_{2FeO} = -528 + 0.1292\,T \ \ \text{kJ mol}^{-1}\qquad(5.1.16)$$

$$\Delta G^o_{SiO_2} = -904.8 + 0.1738\,T \ \ \text{kJ mol}^{-1}\qquad(5.1.17)$$

$$\Delta G^o_{\frac{1}{2}Fe_2SiO_4} = -728.31 + 0.1582\,T \ \ \text{kJ mol}^{-1}\qquad(5.1.18)$$

where T is temperature (°C).

Thus

$$\Delta G_1 < \Delta G_1{}^o - \Delta G_{2\text{FeO}}^o \qquad (5.1.19)$$

$$= -1832.8 + 0.361\,T \qquad (5.1.20)$$

$$< 0, \qquad f \quad T < 5077 \qquad (5.1.21)$$

Since the formation energy ΔG_1 for reaction (5.1.11) is negative, it can be said that Fe_2SiO_4 is more stable than SiO_2 for given conditions.

5.2 Prediction of Oxides Growth

5.2.1 Growth of FeO

The growth of FeO has been investigated by many researchers (Darken and Gurry, 1946; Cabrera and Mott, 1949; Wagner, 1951; Wagner, 1956; Paidassi, 1958; Mrowec, 1967; Yurek *et al.*, 1974; Garnaud and Rapp, 1977; Atkinson, 1982).

Being charged particles, ions will respond to both chemical and electrical-potential gradients, which together provide the net driving force for ion migration. A particle, i, carrying a charge, Z_i, in a position where the chemical-potential gradient is $\frac{d\mu_i}{dz}$ and the electrical-potential gradient is $\frac{d\varphi}{dz}$, is acted on by a force given by equation (5.2.1):

$$\frac{1}{N_A}\left(\frac{d\mu_i}{dz} + Z_i F \frac{d\varphi}{dz}\right) \quad \text{kJ particle}^{-1}\,\mu\text{m}^{-1} \qquad (5.2.1)$$

where N_A is Avogadro`s number F is the Faraday constant in coulombs equiv[-1]. The application of a force to a particle i leads to a velocity, v_i, which is proportional to the acting force, hence for the force in equation (5.2.1),

$$v_i = -\frac{B_i}{N_A}\left(\frac{d\mu_i}{dz} + Z_iF\frac{d\varphi}{dz}\right) \mu m\ s^{-1} \qquad (5.2.2)$$

where B_i is the particle mobility and is defined as the average velocity per unit force, particle. The negative sign in the equation arises since the velocity takes place in the positive z direction for negative chemical and electrical potential gradients. The flux of particles is obtained as equation (5.2.3),

$$j_i = C_iv_i = -\frac{C_iB_i}{N_A}\left(\frac{d\mu_i}{dz} + Z_iF\frac{d\varphi}{dz}\right) mol\ \mu m^{-2}\ s^{-1} \qquad (5.2.3)$$

where C_i is the concentration of i in mol μm^{-3}.

The mobility may be related to the conductivity κ_i and the self diffusion coefficient D_i^* of the particle. The relationships in equation (5.2.4) exist,

$$D_i^* = B_ik_BT = \frac{RT\kappa_i}{C_i(Z_iF)^2} \qquad (5.2.4)$$

where k_B is Boltzmann`s constant.

Writing Z_c and Z_e for the charges on cations and electrons respectively, the condition for electrical neutrality is given by equation (5.2.5).

$$Z_cj_c + Z_ej_e = 0 \qquad (5.2.5)$$

The ionization of a metal M is represented by

$$M = M^{Z_c+} + Z_ce \qquad (5.2.6)$$

And it follows that, at equilibrium, we have the relation given in (5.2.7):

$$\mu_M = \mu_c + Z_c\mu_e \tag{5.2.7}$$

Thus, equation (5.2.8) is obtained:

$$j_c = -\frac{\kappa_c\kappa_e}{(Z_CF)^2(\kappa_c+\kappa_e)}\frac{d\mu_M}{dz} \tag{5.2.8}$$

In general, it is found that the transport number of electrons is close to unity, compared with the transport numbers of cations which is negligibly small. Then equation (5.2.8) becomes

$$j_c = -\frac{\kappa_c}{(Z_CF)^2}\frac{d\mu_M}{dz} \tag{5.2.9}$$

For phases with small deviations from stoichiometry, j_c can be assumed to be independent of z. Then by integrating equation (5.2.8) from the metal-oxide interface to the metal-gas/other oxide interface, equation (5.2.9) is obtained:

$$\int_0^z j_c\ dz = -\frac{1}{(Z_CF)^2}\int_{\mu_M'}^{\mu_M''}\kappa_c\ d\mu_M \tag{5.2.9}$$

where μ_M' is the metal chemical potential at metal - oxide interface and μ_M' is the metal chemical potential at oxide - gas/other oxide interface.
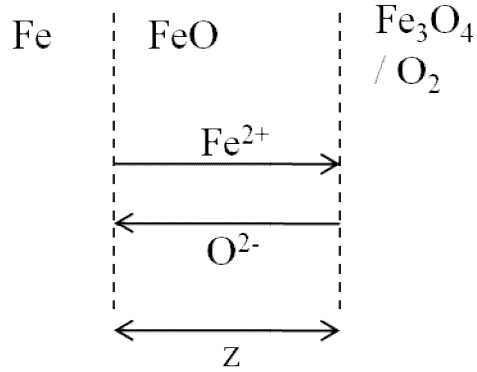
Fig. 5.2.1. A schematic diagram for growth of FeO according to Wagner`s model. Dashed lines present the interface between phases. z indicates the thickness of FeO. Arrows indicate the migration of Fe and O.

A schematic diagram for growth of FeO is in Fig. 5.2.1. The growth of FeO was found to be controlled by outward migration of cation, Fe^{2+}. Also, if the concentration of metal in the oxide is C_M mol cm^{-3} then the flux may also be expressed by equation (5.2.10),

$$j_c = C_M \frac{dz}{dt} \tag{5.2.10}$$

Then, the parabolic rate of FeO, k_{FeO} can be obtained by the definition of equation (2.3.3).

$$k_{FeO} = \frac{1}{C_{Fe}(Z_{Fe^{2+}}F)^2} \int_{\mu_{Fe}'}^{\mu_{Fe}''} \kappa_{Fe^{2+}} \ d\mu_{Fe} \tag{5.2.11}$$

Using equation (5.2.3), we obtain equation (5.2.12).

$$k_{\text{FeO}} = \frac{1}{RT} \int_{\mu_{Fe}'}^{\mu_{Fe}''} D_{\text{Fe}^{2+}}^* \, d\mu_{Fe} \quad \mu\text{m}^{-2} \, \text{s}^{-1} \qquad (5.2.12)$$

Here, $D_{\text{Fe}^{2+}}^*$ is the self diffusion of the cation, Fe^{2+}.

Equation (5.2.13) and (5.2.14) holds thermodynamically.

$$d\mu_{Fe} = RTd\ln a_{Fe} \qquad (5.2.13)$$

$$d\ln a_{Fe} + d\ln a_O = 0 \qquad (5.2.14)$$

Here, a_O is the activity of O. Also, the equation (5.2.15) holds approximately.

$$\ln a_O = \frac{1}{2}\ln P_{O_2} \qquad (5.2.15)$$

Then,

$$k_{\text{FeO}} = \frac{1}{2} \int_{\ln P_{O_2}'}^{\ln P_{O_2}''} D_{\text{Fe}^{2+}}^* \, d\ln P_{O_2} \qquad (5.2.16)$$

The self diffusion coefficient, $D_{\text{Fe}^{2+}}^*$ can be considered as the diffusion coefficient of Fe in FeO, D_{Fe}^{FeO}. The valued for D_{Fe}^{FeO} was obtained from the literature (Chen and Peterson, 1975).

$$D_{\text{Fe}}^{FeO} = 8.6 \times 10^{-3}\exp\left(\frac{-122.80 \text{ kJ mol}^{-1}}{RT}\right) \qquad (5.2.17)$$

$$= 0.0776 \ \mu\text{m}^2 \ \text{s}^{-1} \text{ at } 1000 \ °\text{C}$$

$$= 0.5226 \ \mu\text{m}^2 \ \text{s}^{-1} \text{ at } 1250 \ °\text{C}$$

In the literature (Darken and Gurry, 1946; Cabrera and Mott, 1949; Wagner, 1951; Wagner, 1956; Paidassi, 1958; Mrowec, 1967; Yurek *et al.*, 1974; Garnaud and Rapp, 1977; Atkinson, 1982), the calculations were done with the assumption that FeO grows between substrate and Fe_3O_4. Then equation (5.2.16) became as

$$k'_{FeO} = \frac{1}{2} \int_{\mathbb{h}\, P'_{O_2}}^{\mathbb{h}\, P''_{O_2}} D_{Fe}^{FeO} \; d\ln P_{O_2} \qquad (5.2.16)$$

where k'_{FeO} is the parabolic growth rate of FeO which grows between steel and Fe_3O_4. P'_{O_2} is the equilibrium partial oxygen pressure at the interface between Fe and FeO and P'_{O_2} is the partial oxygen pressure at the interface between FeO and Fe_3O_4. It was confirmed that the growth of FeO is not dependent on the oxygen pressure in atmosphere by experimentally (Pettit and Wagner Jr, 1964; Adachi and Meier, 1987).

The values, P'_{O_2} and P''_{O_2}, were obtained from SSUB4 database with ThermoCalc as seen in Fig. 5.2.2.
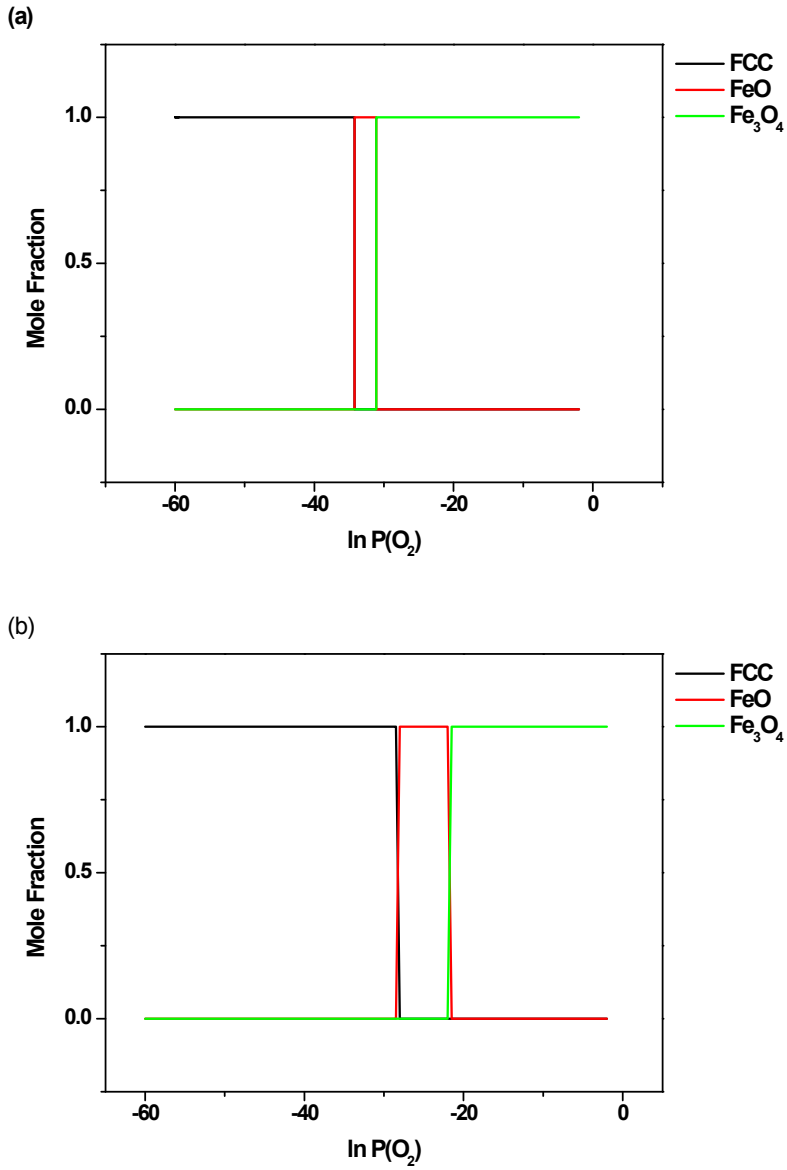
Fig. 5.2.2 The equilibrium mole fractions obtained from SSUB4 database depending on the oxygen pressure at (a) 1000 °C and (b) 1250 °C. Black, red and green lines indicate FCC austenite, FeO and Fe$_3$O$_4$, respectively.

Temp. / °C	$\ln P'_{O_2}$/atm	$\ln P'_{O_2}$/atm
1000	-34.2385	-31.0880
1250	-26.0767	-21.4736

Table 5.2.1 The values for $\boldsymbol{P'_{O_2}}$ and $\boldsymbol{P'_{O_2}}$ obtained from SSUB4 database

Then,

$$k'_{FeO} = 0.1223 \ \mu m^2 \ s^{-1}, \text{ at 1000 °C}$$

$$= 1.2029 \ \mu m^2 \ s^{-1}, \text{ at 1250 °C}$$

In most cases, FeO was assumed to grow between steel and Fe_3O_4 since Fe_3O_4 is stable at the higher oxygen pressure than that of FeO as seen in Fig. 5.2.1. The thickness of FeO can be calculated by equation (2.3.4) and the results are shown in Fig. 5.2.3.
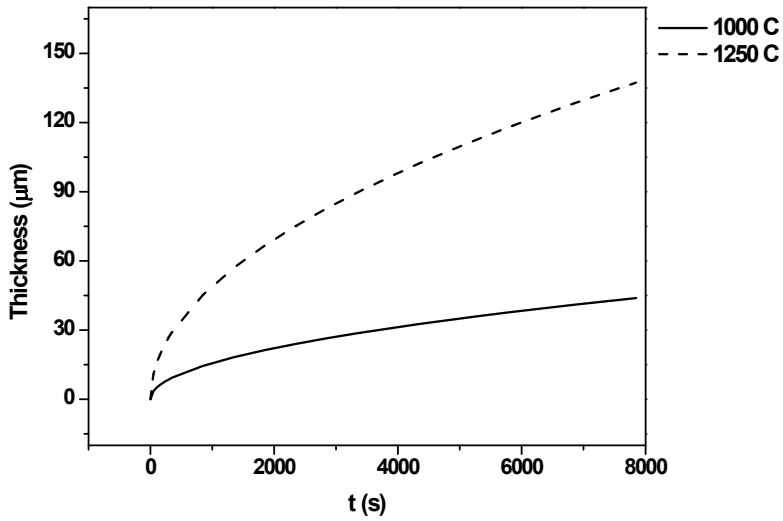
Fig. 5.2.3 The calculated thickness of FeO growing between substrate and Fe_3O_4. Solid line and dashed line represent that of FeO at 1000 ºC and 1250 ºC, respectively.

Suppose FeO forms between substrate and gas. Then, equation (5.2.16) became as

$$k'_{FeO} = \frac{1}{2} \int_{h\,P'_{O_2}}^{h\,P''_{O_2}} D_{Fe}^{FeO} \, d\ln P_{O_2} \qquad (5.2.16)$$

where k'_{FeO} is the parabolic growth rate of FeO which grows between steel and O_2. P'_{O_2} is the equilibrium partial oxygen pressure at the interface between Fe and FeO and P'_{O_2} is the partial oxygen pressure at the interface between FeO

48

and O_2 gas. Here, the same value in equation (5.2.14) was used for P'_{O_2} and partial oxygen pressure in air, 0.2 atm, was used for P''_{O_2}.

Then,

$$k'_{FeO} = 1.2669 \ \mu m^2 \ s^{-1}, \text{ at } 1000 \ ^\circ C$$
$$= 6.3937 \ \mu m^2 \ s^{-1}, \text{ at } 1250 \ ^\circ C$$

5.2.2 Growth of Fe$_2$SiO$_4$ and SiO$_2$

Oxides formed on Fe – 1.5 Si wt% steel at 1000 °C exposed to carbon dioxide and carbon monoxide atmospheres have previously been investigated. The amorphous silica film formed on the specimens and crystallized to β-cristobalite at the reaction temperature. FeO and Fe$_2$SiO$_4$ developed within nodules which grew laterally to cover the alloy surface. Concurrent with growth of the nodules on the steel surface, oxygen diffusion into the underlying alloy led to precipitation of silica as α-tridymite. A fully developed scale was composed of an external wüstite layer and an inner FeO – Fe$_2$SiO$_4$ conglomerate layer, interspersed with discontinuous Fe$_2$SiO$_4$ bands. (Logani and Smeltzer, 1969; Logani and Smeltzer, 1971). However, in the study oxides including SiO$_2$ were assumed to form on the surface of the substrate in order to reduce the surface energy, maximize the oxygen supply, and simplify the problem.

Since migration of oxygen into the substrate is much faster than migration of silicon, rate-controlling step for growth of SiO_2 and Fe_2SiO_4 could be the outward diffusion of silicon. A schematic diagram for formation of Fe_2SiO_4 and SiO_2 is in Fig. 5.2.4.
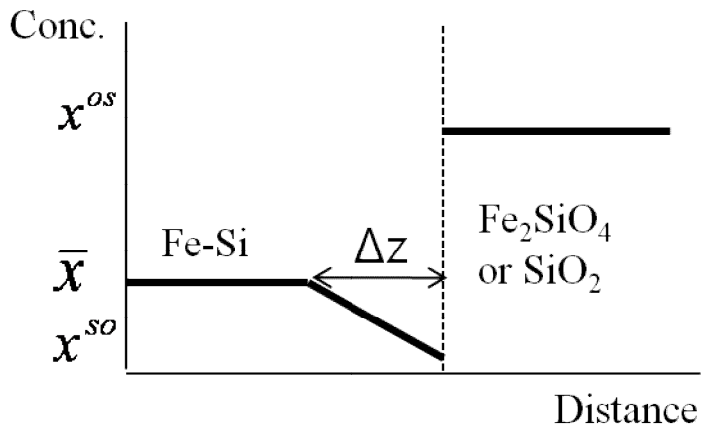

Fig. 5.2.4 The schematic diagram for the formation of Fe_2SiO_4 and SiO_2. The dashed line presents the interface between austenite and the oxide. x^{os} and x^{so} is the equilibrium silicon concentration in the oxide and steel, respectively. $\bar{x}$ is the average silicon concentration near the steel surface.

Following equations can predict the growth of those oxides,

$$(x^{os} - x^{so})\frac{dz}{dt} = D_{si}\frac{\bar{x} - x^{so}}{\Delta z}$$ (5.2.20)

$$\frac{1}{2}\Delta z(\bar{x} - x^{so}) \fallingdotseq z(x^{os} - \bar{x})$$ (5.2.21)

where t is the growth time, x^{os} is the silicon concentration in oxide, x^{so} is the silicon concentration in steel in equilibrium with oxide, $\bar{x}$ is the average silicon concentration near the steel surface, D_{si} is the diffusivity of silicon in the substrate, z is the position of interface between steel and oxide.

Then,

$$\frac{dz}{dt} = \frac{D_{si}\ (\bar{x} - x^{so})^2}{2z(x^{os} - x^{so})(x^{os} - \bar{x})}$$ (5.2.22)

Thus by the definition in equation (2.3.3), the parabolic growth rate of SiO_2 or Fe_2SiO_4 can be written as

$$k = \frac{D_{si}\ (\bar{x} - x^{so})^2}{2(x^{os} - x^{so})(x^{os} - \bar{x})}$$ (5.2.23)

These equations can only be applied if $0 < \bar{x} \leq x^{os}$ because silicon concentration of substrate should be smaller than that of oxides in order to explain the mechanism with the diffusion of silicon.

For both SiO_2 and Fe_2SiO_4, TCFE6 and SSUB4 database with ThermoCalc was used for the weight fraction of silicon in steel in equilibrium with oxides

and the results were $x^{so} = 10^{-12}$. It is reasonable since the formation energy of SiO$_2$ and Fe$_2$SiO$_4$ is very low. The weight fraction of silicon in oxides, x^{os} are 0.4667 and 0.1429 for SiO$_2$ and Fe$_2$SiO$_4$, respectively.

The diffusion coefficients of silicon in FCC austenite and BCC ferrite were obtained from MOBFE1 database with DICTRA.

Temp. / °C	D_{Si}^{α} / μm^2 s^{-1}	D_{Si}^{γ} / μm^2 s^{-1}
1000	0.11134	8.5802×10^{-4}
1250	5.0719	0.03656

Table 5.2.2 The values for $\boldsymbol{D_{Si}^{\alpha}}$ and $\boldsymbol{D_{Si}^{\gamma}}$ obtained from MOBFE1 database

The calculated results are shown in Fig. 5.2.5. According to the equation (5.2.23), the growth rate of Fe$_2$SiO$_4$ is always faster than that of SiO$_2$. It is reasonable because the condition for formation of Fe$_2$SiO$_4$ can meet much easier if $0 < \bar{x} \leq x^{os}$. The rapid increase in the growth rate for Fe – 0.1 C – 1.9 Si wt% steel and Fe – 0.1 C – 2.9 Si wt% steel at 1000 ºC and 1250 ºC was caused by the change of substrate from FCC austenite to BCC ferrite.
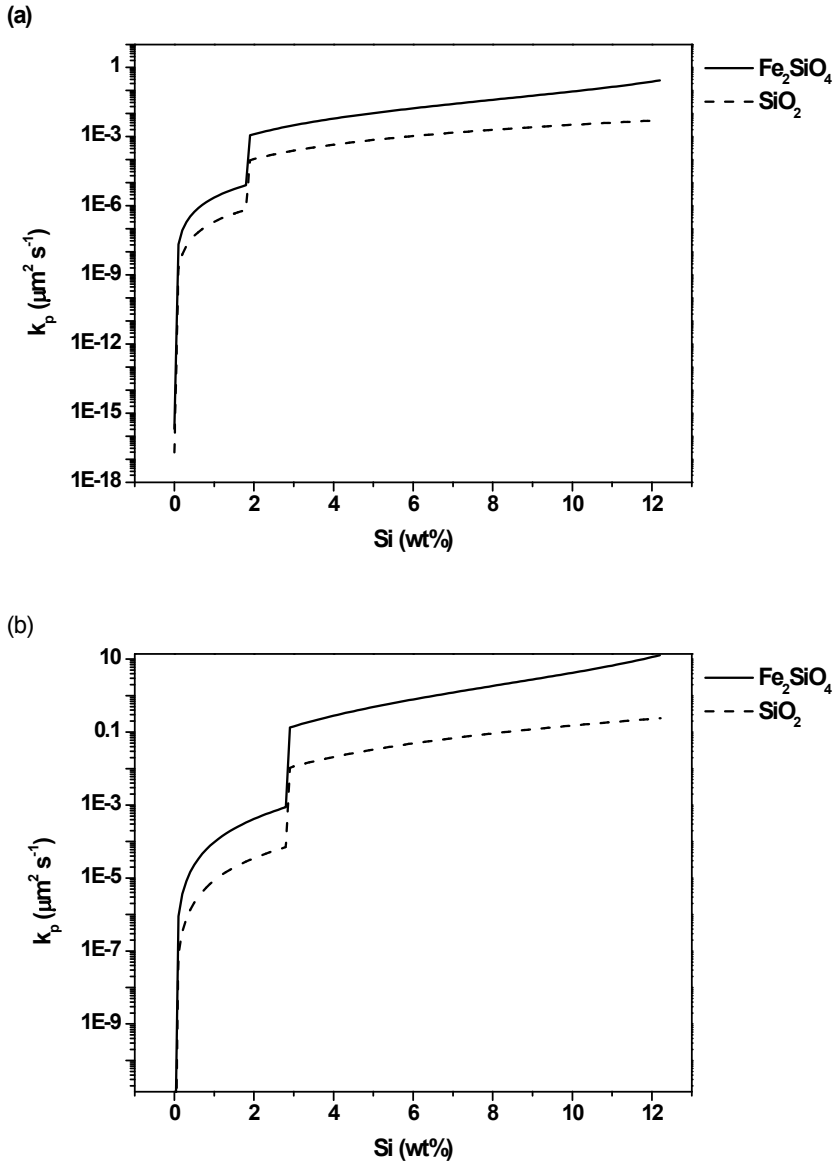
(a)

(b)

Fig. 5.2.5 The calculated growth rate of SiO_2 and Fe_2SiO_4 of $Fe - 0.1\ C - (0 \sim 12)$ Si wt% steel at (a) 1000 ºC and (b) 1250 ºC. Solid and dashed lines present the parabolic growth rate of Fe_2SiO_4 and SiO_2, respectively.

5.3 Prediction of Simultaneous Oxides

Since the formation of oxides happen concurrently, it should be considered simultaneously. In this study, the growth of SiO_2, Fe_2SiO_4 and FeO was considered because the main interest is the red-scale caused by Fe_2SiO_4.

There are two factors to consider in the simultaneous growth of those oxides. First, the area which oxides could form is limited as the area of the substrate. Thus the modified concepts of extended area were used (Christian, 1975; Bhadeshia, 1999) .

There is another factor to be considered in the simultaneous formation of SiO_2, Fe_2SiO_4 and FeO. The growth rate of FeO is much larger than diffusivity of silicon. For example, at 1000 ℃, $k'_{FeO} = 1.2669$ μm^2 s^{-1} and $D_{Si}^{\gamma} = 8.58 \times 10^{-4}$ μm^2 s^{-1}. Hence silicon concentration in substrate near the interface between substrate and oxides might be higher than the average silicon concentration in steel. However this factor is not considered in this study.

Suppose SiO_2, Fe_2SiO_4 and FeO nucleate at the substrate surface and grow both laterally and vertically in the hemisphere shape. It should be noted that the vertical growth of oxides is only allowed until the substrate surface is fully covered with oxides.

For SiO_2 and Fe_2SiO_4, the mechanism for the lateral growth and vertical growth is same. They both happen at the interface between the substrate and the oxide.

Since the growth rates of SiO_2 and Fe_2SiO_4 were calculated with the assumption on the substrate/oxide interface movement, the lateral diameter r^l and the vertical diameter r^v follow the parabolic growth rate obtained in previous chapter.
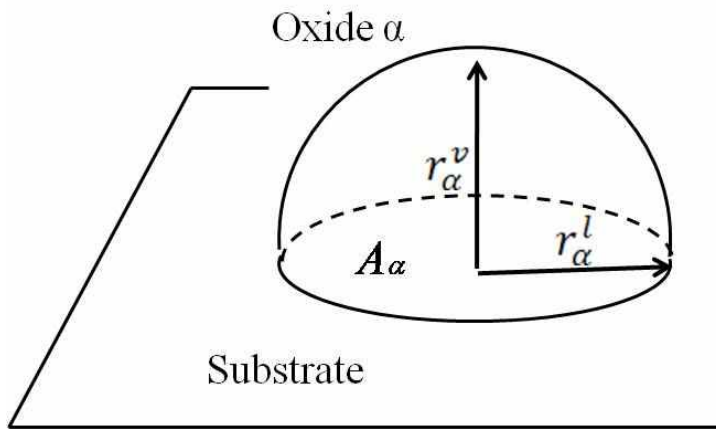

Fig. 5.3.1 The schematic diagram of growth of SiO_2 and Fe_2SiO_4 on the substrate. If the oxide is indicated α, A_α represents the area of oxide α which meets the substrate surface. The oxide α is assumed to grow in the hemisphere shape. The lateral diameter r^l_α and the vertical diameter r^v_α follow the parabolic growth rate k_α, which is calculated from the movement of the substrate/oxide interface.

However, the mechanism for FeO is different. The lateral growth happens at the interface between the substrate and FeO while the vertical growth happens at the

interface between FeO and O_2. In the previous chapter, the growth rate was calculated based on the migration of Fe. However, in that case the growth of FeO means the movement of FeO/O_2 interface not steel/FeO interface. Thus the growth rate calculated in the previous chapter based on the migration of Fe cannot predict the lateral growth but only the vertical growth. For the lateral growth, the growth rate needs to be calculated based on the migration of oxygen. If we substitute cation to anion in equation (5.2.12), equation (5.3.1) is obtained.

$$k_{FeO}^O = \frac{1}{RT} \int_{\mu_O'}^{\mu_O''} D_{O^{2-}}^* \ d\mu_O \quad \mu m^{-2} \ s^{-1} \qquad (5.3.1)$$

Here, μ_O' is the oxygen chemical potential at Fe/FeO interface and μ_O' is the oxygen chemical potential at FeO/O_2 interface.

Thermodynamically, equation (5.3.2) holds.

$$d\mu_O = RTd\ln a_O \qquad (5.3.2)$$

Then the growth rate of FeO based on migration of oxygen k_{FeO}' can be obtained from equation (5.3.3).

$$k_{FeO}^O = \frac{1}{2} \int_{h \ P_{O_2}'}^{h \ P_{O_2}''} D_{O^{2-}}^* \ d\ln P_{O_2} \quad \mu m^{-2} \ s^{-1} \qquad (5.3.3)$$

Here, P_{O_2}' is the equilibrium partial oxygen pressure at the interface between Fe and FeO, P_{O_2}'' is the partial oxygen pressure at the interface between FeO and O_2. Also, $D_{O^{2-}}^*$ is the self diffusion coefficient of the anion, O^{2-}. Here, the same value in equation (5.2.14) can be used for P_{O_2}' and partial oxygen pressure in air, 0.2 atm, can be used for P_{O_2}''. The self diffusion coefficient of $D_{O^{2-}}^*$ can be

considered as the diffusion coefficient of oxygen in FeO, D_O^{FeO}. The value for D_O^{FeO} at 1000 °C was obtained from the literature (Millot, 1997).

$$D_O^{FeO} = 6.1660 \times 10^{-6} \ \mu m^2 \ s^{-1}, \text{at } 1000 \text{ °C}$$

Then,

$$k_{FeO}^O = 1.001 \times 10^{-4} \ \mu m^2 \ s^{-1}, \text{at } 1000 \text{ °C}$$

However, the value for D_O^{FeO} at 1250 °C was not found. Thus k_{FeO}^O at 1250 °C could not be obtained in this study.

Let the area of SiO_2, Fe_2SiO_4, FeO and the substrate be A_{SiO_2}, $A_{Fe_2SiO_4}$, A_{FeO} and A_s. In this case, A_s is the total area. Also, let the extended area of SiO_2, Fe_2SiO_4 and FeO be $A_{SiO_2}^e$, $A_{Fe_2SiO_4}^e$ and A_{FeO}^e. Suppose that the nucleation sites are formed only at $t=0$ and the nucleation sites per unit area of SiO_2, Fe_2SiO_4 and FeO are N_{SiO_2}, $N_{Fe_2SiO_4}$ and N_{FeO}, respectively. Here the unit of nucleation rate is μm^{-2}.

Then at time t,

$$A_{SiO_2}^e = \pi \, 2k_{SiO_2} t \, N_{SiO_2} \ A_s \qquad (5.3.1)$$

$$A_{Fe_2SiO_4}^e = \pi \, 2k_{Fe_2SiO_4} t \, N_{Fe_2SiO_4} \ A_s \qquad (5.3.2)$$

$$A_{FeO}^e = \pi \, 2k_{FeO}^O \, t \, N_{FeO} \ A_s \qquad (5.3.3)$$

The change in the area of oxides can be obtained as

$$dA_{SiO_2} = \left(1 - \frac{A_{FeO}}{A_s} - \frac{A_{SiO_2}}{A_s} - \frac{A_{Fe_2SiO_4}}{A_s}\right) d \, A_{SiO_2}^e \qquad (5.3.4)$$

$$dA_{Fe_2SiO_4} = \left(1 - \frac{A_{FeO}}{A_s} - \frac{A_{SiO_2}}{A_s} - \frac{A_{Fe_2SiO_4}}{A_s}\right) d\, A^e_{Fe_2SiO_4} \quad (5.3.5)$$

$$dA_{FeO} = \left(1 - \frac{A_{FeO}}{A_s} - \frac{A_{SiO_2}}{A_s} - \frac{A_{Fe_2SiO_4}}{A_s}\right) dA^e_{FeO} \quad (5.3.6)$$

By the initial condition, equation (5.3.7) is obtained.

$$A_{FeO} = A_{SiO_2} = A_{Fe_2SiO_4} = 0, \; f \; t = 0 \quad (5.3.7)$$

Then the ratio between the areas of each oxide is obtained from equation (5.3.8).

$$A_{SiO_2} : A_{Fe_2SiO_4} : A_{FeO}$$

$$= k_{SiO_2} N_{SiO_2} : k_{Fe_2SiO_4} N_{Fe_2SiO_4} : k^O_{FeO} N_{FeO} \quad (5.3.8)$$

After the substrate surface is fully covered with the oxides, oxides are supposed to grow in the cylindrical shape toward the gas which heights follow the calculated growth rate in previous chapter.

The volume of SiO_2, Fe_2SiO_4 and FeO, V_{SiO_2}, $V_{Fe_2SiO_4}$ and V_{FeO} can be obtained as equation (5.3.9), (5.3.10) and (5.3.11).

$$V_{FeO} = A_{FeO}\sqrt{2\,k_{FeO}\,t} \quad (5.3.14)$$

$$V_{SiO_2} = A_{SiO_2}\sqrt{2k_{SiO_2}t} \quad (5.3.15)$$

$$V_{Fe_2SiO_4} = A_{Fe_2SiO_4}\sqrt{2k_{Fe_2SiO_4}t} \quad (5.3.16)$$

Thus the volume fractions of SiO_2, Fe_2SiO_4 and FeO can be obtained as

$$V_{\mathrm{SiO_2}} : V_{\mathrm{Fe_2SiO_4}} : V_{\mathrm{FeO}} =$$

$$N_{\mathrm{SiO_2}} (k_{\mathrm{SiO_2}})^{\frac{3}{2}} : N_{\mathrm{Fe_2SiO_4}} (k_{\mathrm{Fe_2SiO_4}})^{\frac{3}{2}} : N_{\mathrm{FeO}} \, k^O_{FeO} (k_{\mathrm{FeO}})^{\frac{1}{2}} \qquad (5.3.17)$$

If we assume the nucleation rates per unit are of SiO$_2$, Fe$_2$SiO$_4$ and FeO are same and independent of the silicon concentration in steel, volume fractions of oxides on Fe – 0.1 C – (0 ~ 13) Si wt% steel can be obtained as seen in Fig. 5.3.2. Volume fractions for oxides formed on silicon containing steel were calculated according to the equation (5.3.17). However, for 1250 °C, k_{FeO} was used instead of k^O_{FeO} because the value for k^O_{FeO} was not obtained.

At 1000 °C, for oxides on Fe – 0.1 C – (0 ~ 1.9) Si wt% steel which equilibrium phase is FCC, the volume fraction of FeO is almost 1. It is reasonable because the diffusion of Fe in FeO is much greater than the diffusion of Si in austenite. As increasing the silicon concentration in steel, BCC ferrite becomes stable thus volume fraction of Fe$_2$SiO$_4$ and SiO$_2$ could be increased rapidly because of the large diffusivity in BCC ferrite. However, the volume fraction of Fe$_2$SiO$_4$ is much larger than that of SiO$_2$ for Fe – 0.1 C – (0 ~ 13) Si wt% steel. It can be explained the growth rate of Fe$_2$SiO$_4$ is much faster than SiO$_2$ as seen in Fig. 5.2.4. For the steel containing more than 1.9 wt% silicon, BCC ferrite is stable at 1000 °C as seen in Fig. 5.1.1.Thus silicon could diffuse faster and cause rapid increase in the volume fraction of SiO$_2$ and Fe$_2$SiO$_4$.
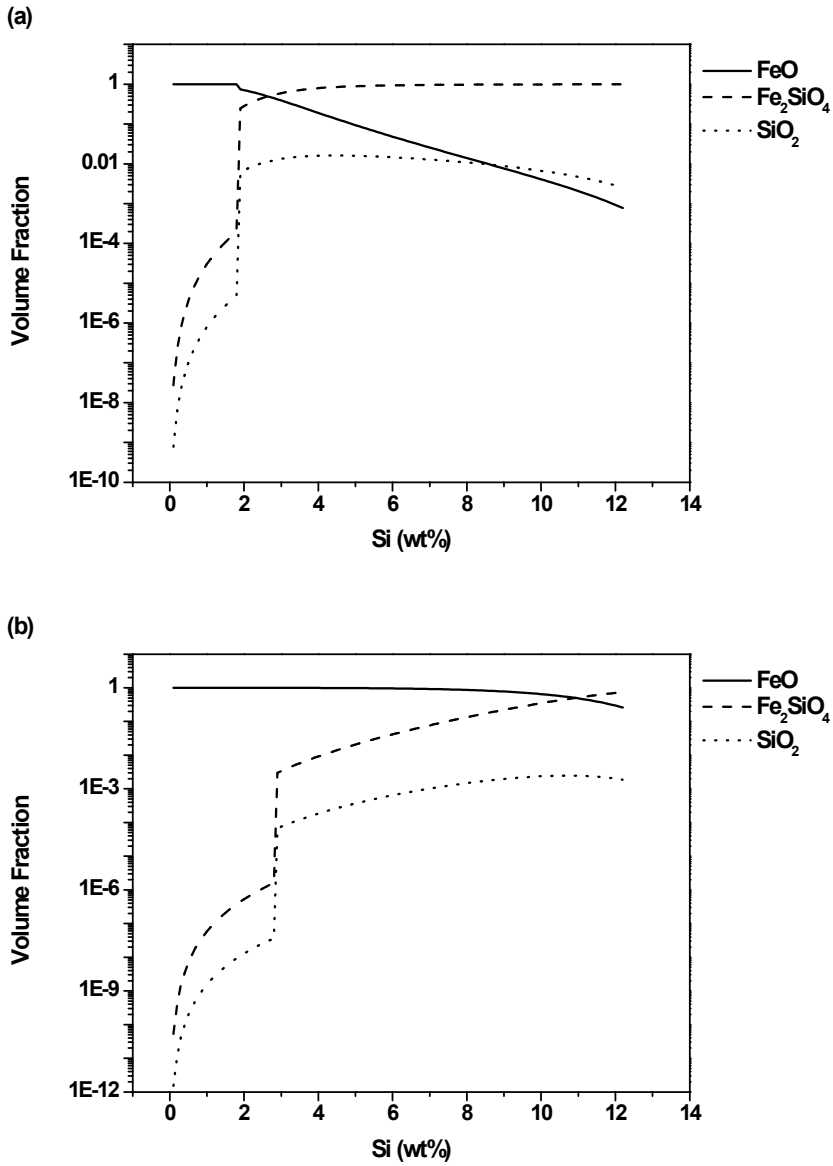
Fig. 5.3.2 Volume fractions for oxides formed on Fe – 0.1 C – (0 ~ 13) Si wt% steel at (a) 1000 °C and (b) 1250 °C. Solid, dashed and dot lines indicate volume fractions of FeO, Fe₂SiO₄ and SiO₂, respectively.

The nucleation rates per unit area of SiO_2, Fe_2SiO_4 and FeO; N_{SiO_2}, $N_{Fe_2SiO_4}$ and N_{FeO} could be obtained as follows. The free energy change associated with the nucleation of oxide α has three contributions.

(1) A temperatures where an oxide α is stable, the creation of a volume V_α of α will cause a volume free energy reduction of $V_\alpha \Delta G_\alpha^V$.

(2) Assuming that the steel/oxide interfacial energy, γ_{so} is isotropic of the area meeting the substrate, A_1 of interface, free energy will increase by $A_1 \gamma_{so}$.

(3) Assuming that the oxide surface energy, γ_o is isotropic of the surface area, A_2, free energy will increase by $A_2 \gamma_o$.

Summing all of these gives the total free energy change as

$$\Delta G = -V_\alpha \Delta G_\alpha^V + A_1 \gamma_{so} + A_2 \gamma_o \tag{5.3.9}$$

Since the nuclei of oxides are assumed to grow in the hemisphere shape with diameter, r, equation (5.3.10) can be obtained.

$$\Delta G = -\frac{2}{3}\pi r^3 \Delta G_V + \pi r^2 \gamma_{so} + 2\pi r^2 \gamma_o \tag{5.3.10}$$

Differentiation of equation (5.3.11) yields maximum excess free energy, ΔG^*, and its radius, r^*.

$$r^* = \frac{\gamma_{so} + 2\gamma_o}{\Delta G_V} \tag{5.3.11}$$

$$\Delta G^* = -\frac{2}{3}\pi(r^*)^3 \Delta G_V + \pi(r^*)^2 \gamma_{so} + 2\pi(r^*)^2 \gamma_o \qquad (5.3.12)$$

The formation of nuclei is assumed to happen only at $t=0$. Then the number of cluster per unit area that have reached the critical size r^* could be considered as the number of nucleation sites per unit area. Let C_α be the number of atoms per unit area contained in the oxide α. Then, N_α can be obtained from equation

$$N_\alpha = C_\alpha \exp\left(\frac{-\Delta G_\alpha^*}{k_B T}\right) \qquad (5.3.13)$$

In this study, the nucleation rates per unit area of SiO_2, Fe_2SiO_4 and FeO; N_{SiO_2}, $N_{Fe_2SiO_4}$ and N_{FeO} were not calculated. The values for interface energy between steel/oxides and surface energy of oxides need to be obtained.

5.4 Characterization of Oxides

The samples were oxidized at 1000 °C and 1250 °C so as to observe the oxide formation. Fig. 5.4.1 is the OM image of oxides on Alloy 1 formed at 1000 °C for 2 hours. The mixture of FeO and Fe_3O_4, Fe_3O_4, Fe_2O_3 were observed going from substrate to gas. The mixture of FeO and Fe_3O_4 was formed since FeO is not stable under 570 °C and reaction in (2.2.2) could happen. In this study, the cooling rate is 20 ° per a minute, which is slow enough to form Fe_3O_4 from FeO (Chen and Yeun, 2003). Those phases were identified by the quantative analysis of EDS and WDX..
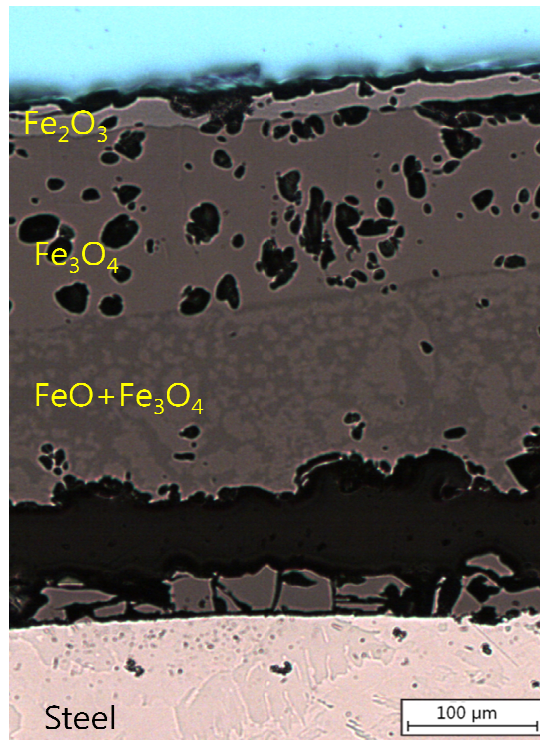
Fig. 5.4.1 OM image of oxides on Alloy1 formed at 1000 °C for 2 h

Fig. 5.4.2 shows the BSE images of oxides formed on Si Alloy 1000 °C for 2 hours. The oxides were composed of Fe_2O_3, Fe_3O_4, and a mixture of FeO and Fe_2SiO_4, going from gas to the substrate. It is known that the FeO layer takes about 95% of the entire oxide. However in this study, it is not because FeO decomposition reaction happened via equation (2.2.2) same as the oxides of Alloy 1. Since the size of Fe_2SiO_4 was less than 700 nm, phases was identified by

TEM EDS. Also, the distribution of each element was obtained by EPMA as seen in Fig. 5.2.3. It is found that if silicon-added steel oxidizes, silicon forms Fe_2SiO_4 as a thin layer at the interface between steel and oxide and does not form SiO_2 in this experimental condition. The volume fraction of all oxides and Fe2SiO4 was about 86 : 14. In the mixture, the phase fraction of FeO and Fe_2SiO_4 was about 46 : 54.
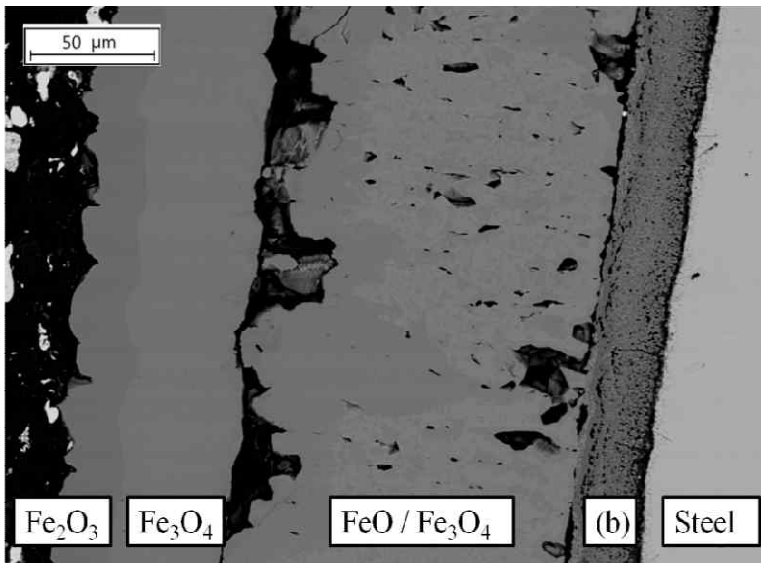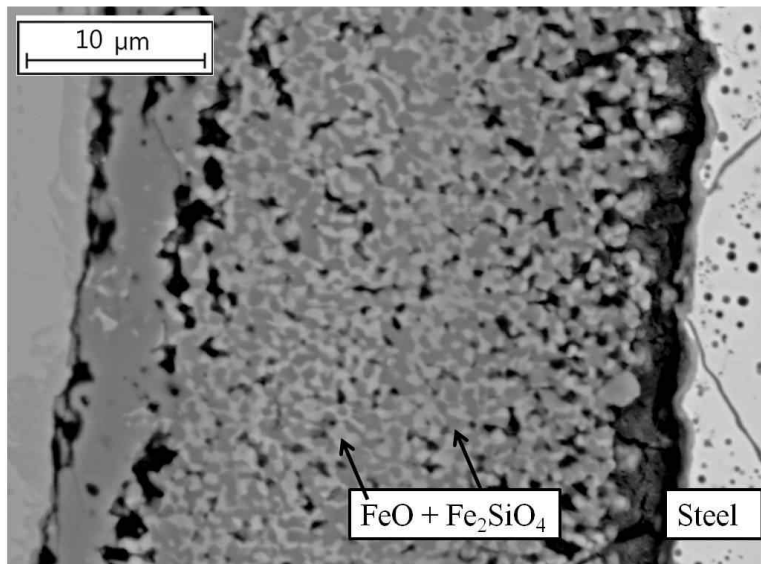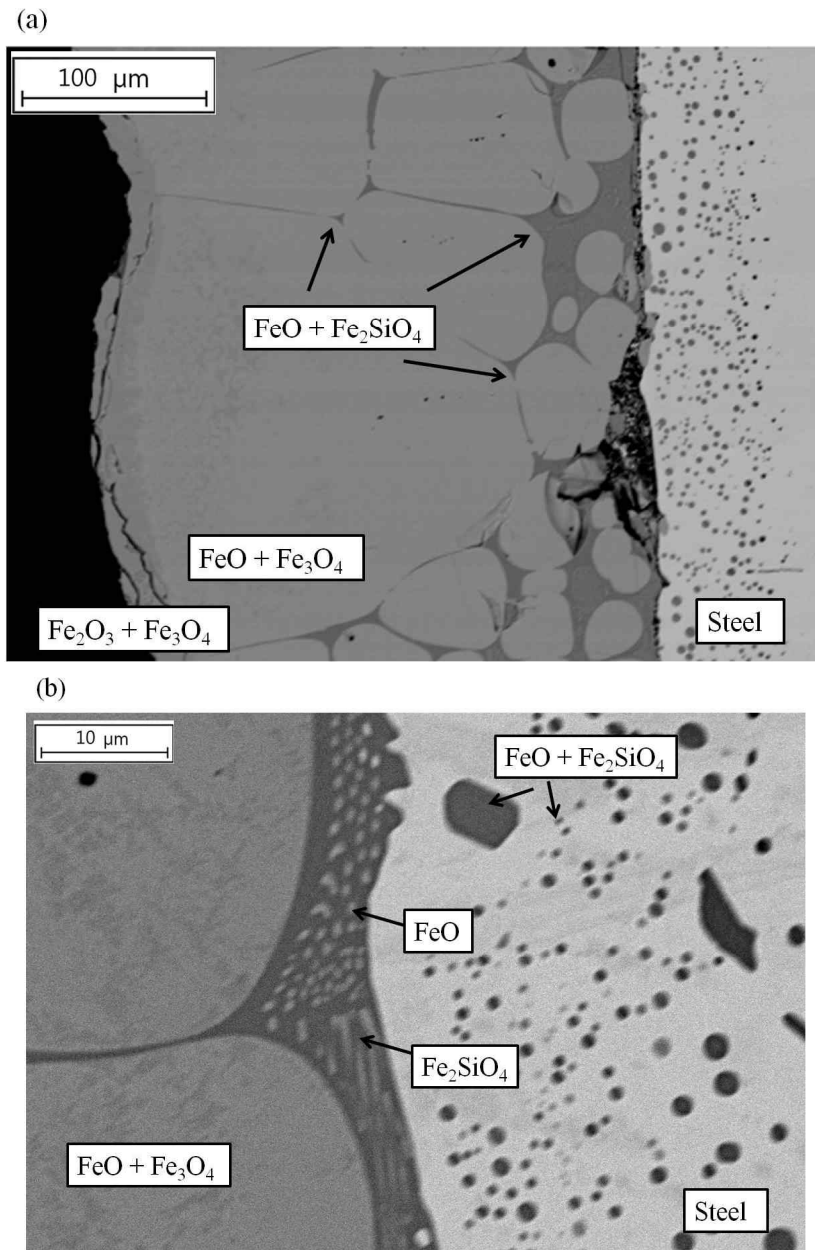
Fig. 5.4.2 BSE images of oxides formed at 1000 ℃ for 2 h of Si Alloy.

(b) shows the oxide formed at interface in high magnification. The bright part is

FeO and dark part is Fe$_2$SiO$_4$ as the arrows indicate.
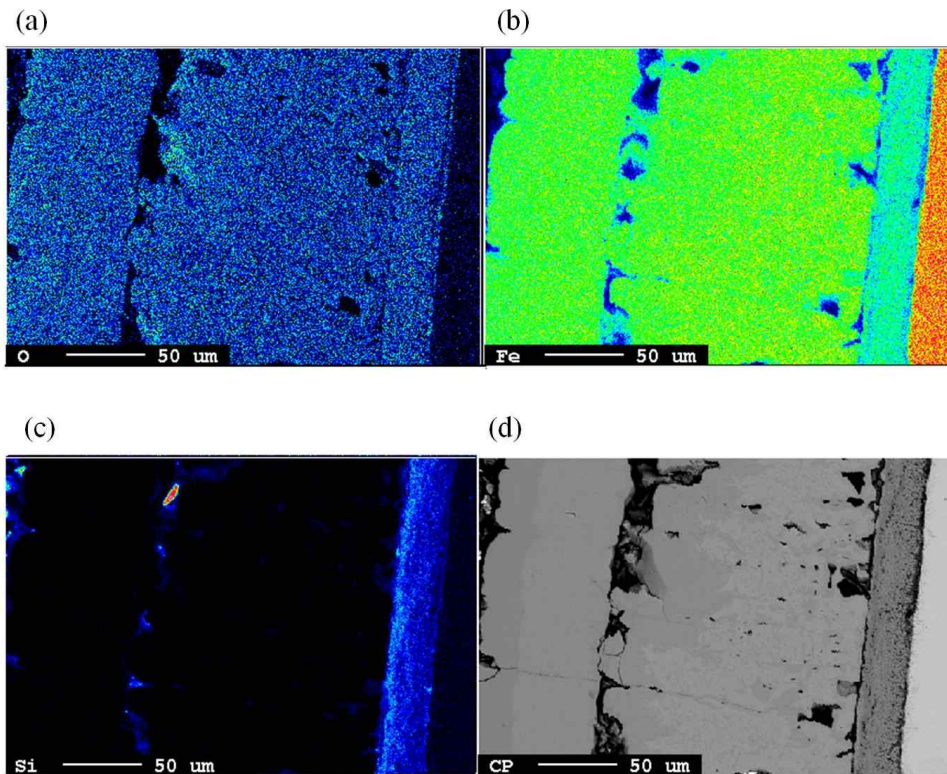
Fig. 5.4.3 EPMA images of oxides formed at 1000 ºC for 2 h of Alloy 2;

(a), (b), (c) indicate O, Fe, Si, respectively.

At 1250 ºC, the eutectic compound of FeO and Fe_2SiO_4 was found. It penetrates into the substrate and FeO. Fig. 5.4.4 show the BSE images of oxides formed at 1250 ºC for 2 hours of Si Alloy. The distribution of each element was obtained by EPMA as seen in Fig. 5.4.5. It is found that if silicon-added steel oxidizes at 1250 ºC, silicon forms the eutectic compound of Fe_2SiO_4 and FeO which

penetrates into grain boundaries of FeO. The volume fraction of all oxides and Fe_2SiO_4 was about 87 : 13. In the mixture, the phase fraction of FeO and Fe_2SiO_4 was about 13 : 87.

To indentify the phases of oxides, XRD analysis was carried out with the oxides formed at at 1250 ºC on Si Alloy. Fig 5.4.6 shows XRD results for those oxides. The bottom part of oxides was powdered before the XRD analysis. The upper part of oxides was removed before the analysis. The green presents the oxides of Si Alloy. Mark W, M and F indicate the phase FeO, Fe_3O_4 and Fe_2SiO_4, respectively. The peaks for FeO, Fe_3O_4 and Fe_2SiO_4 were found but the peaks for SiO_2 was not found in this result.

Fig. 5.4.4 BSE images of oxides formed at 1250 ℃ for 2 h of Si Alloy;

(b) shows the oxide formed at interface in high magnification. The bright part is

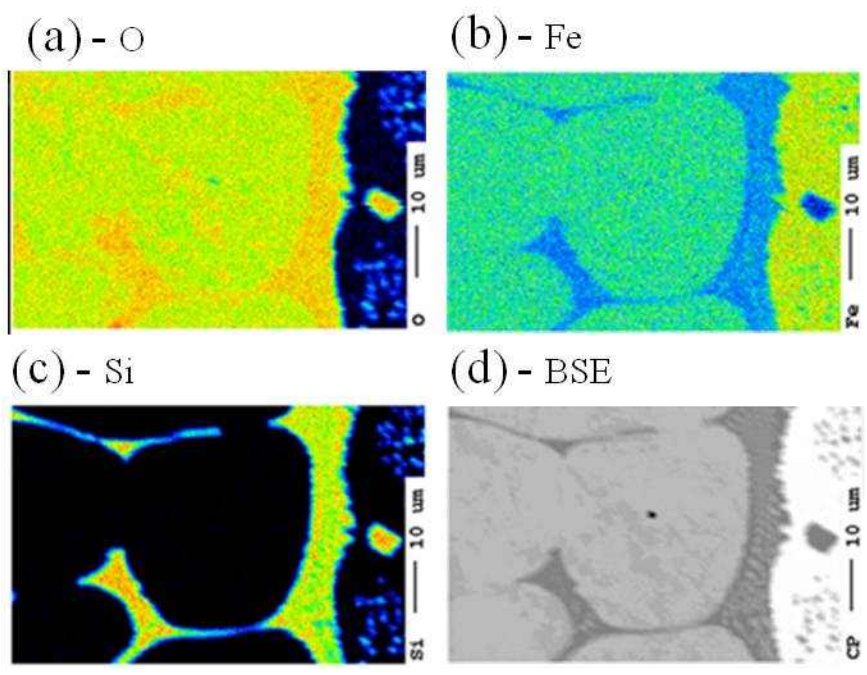FeO and dark part is Fe_2SiO_4 as the arrows indicate.

Fig. 5.4. 5 EPMA images of oxides formed at 1250 ºC for 2 h of Si Alloy;
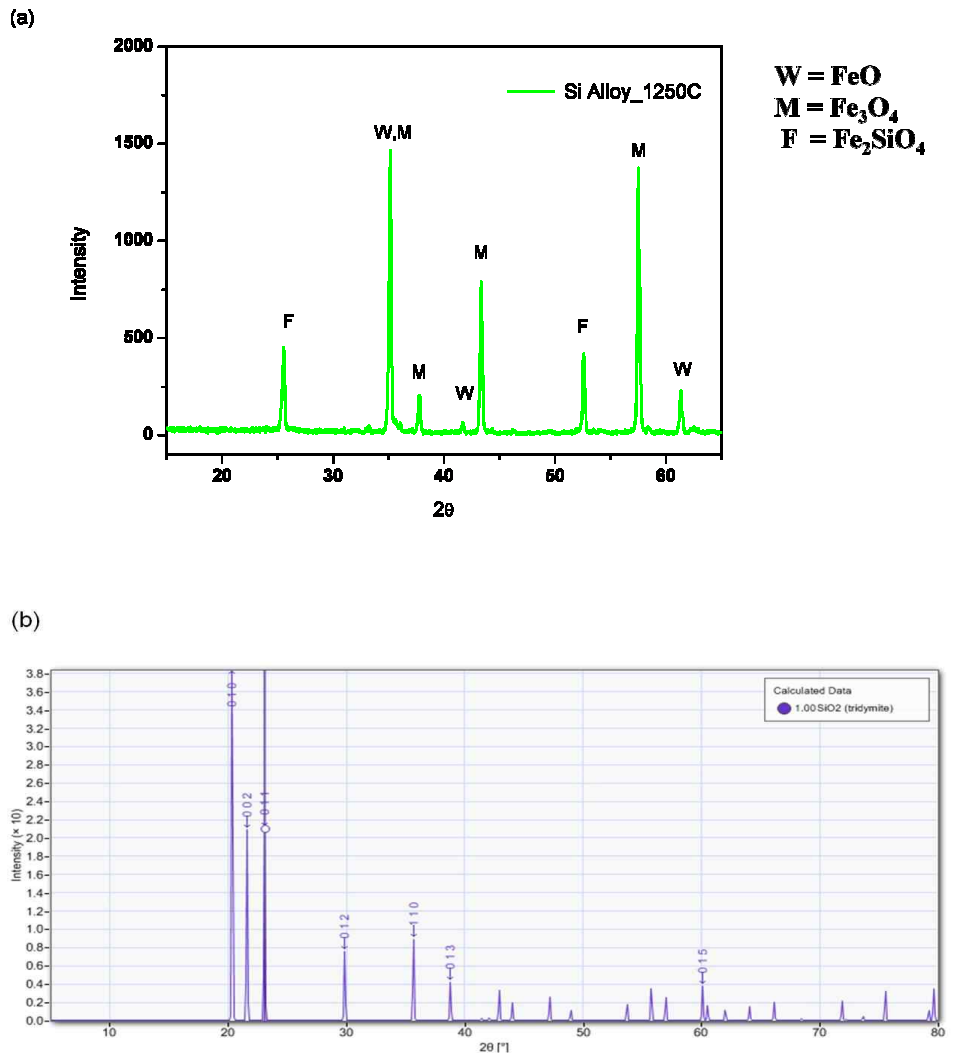
(a), (b), (c) indicate O, Fe, Si, respectively.

(a)

(b)

Fig. 5.4.6 (a) shows XRD results for the oxides formed at 1250 ºC. The black and red line presents the oxides of Alloy 1 and Si Alloy, respectively. The green presents the oxides of Si Alloy. Mark W, M and F indicate the phase FeO, Fe_3O_4 and Fe_2SiO_4, respectively. (b) shows the calculated XRD peaks of SiO_2.

Fig. 5.4.7, Fig. 5.4.8 shows the BSE image of oxides formed on Ni Alloy at 1000 ºC and 1250 ºC, respectively. The distributions of oxides were analyzed with EPMA as seen in Fig. 5.4.9 and Fig. 5.4.10. At the interface between substrate and oxides, there were the layer containing FeO, Fe_2SiO_4 and unoxidized steel. Those steel are indicated with red arrows. Also the interface became more uneven due to the Ni addition. This is in a good agreement with the previous results of other researchers (Fukagawa *et al.*, 1996; Asai *et al.*, 1997).
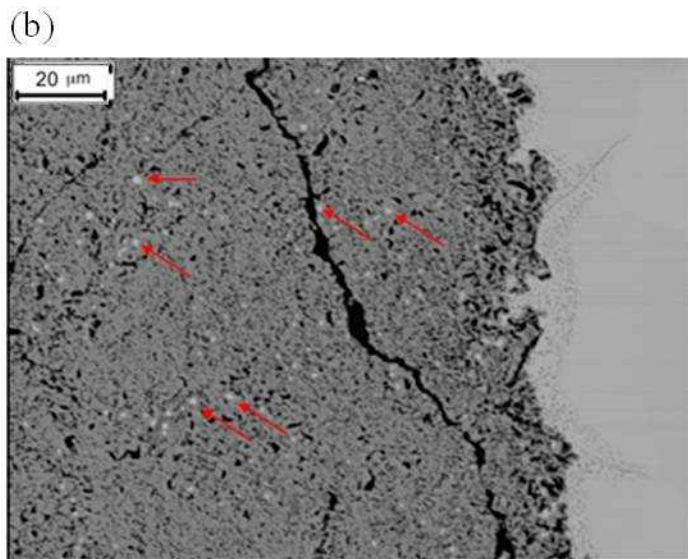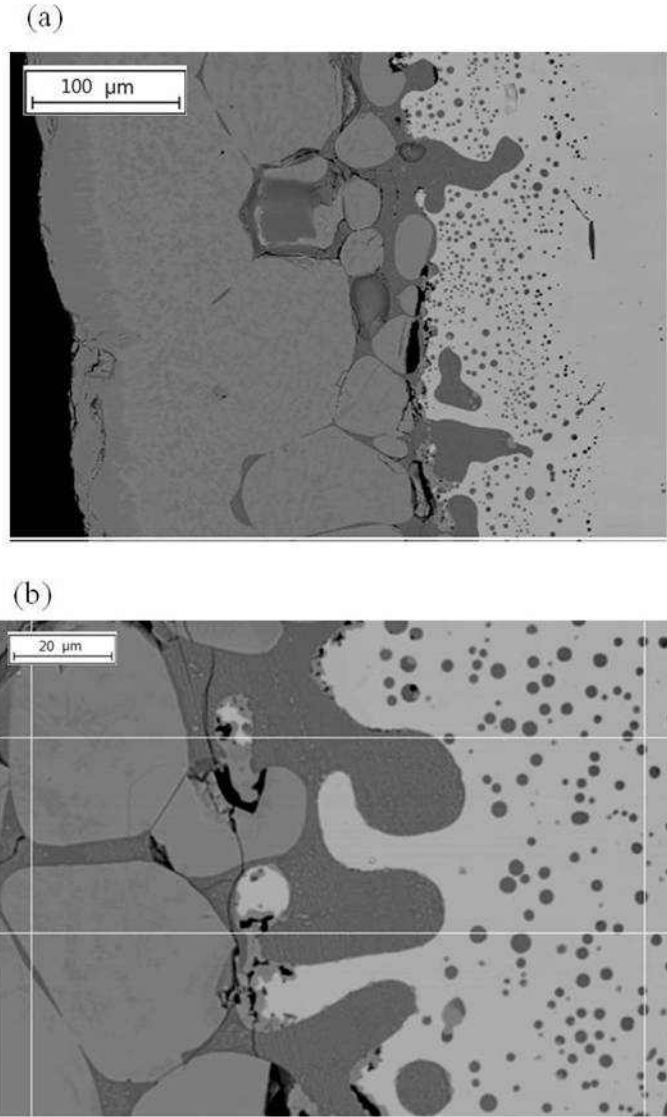
Fig. 5.4.7 BSE images of oxides formed at 1000 ºC for 2 h of Ni Alloy;

(b) shows the oxide formed at interface in high magnification. The bright part is

FeO and dark part is Fe_2SiO_4 and white part is steel as the arrows indicate.

Fig. 5.4.8. BSE images of oxides formed at 1250 ºC for 2 h of Ni Alloy;

(b) shows the oxide formed at interface in high magnification. The bright part is

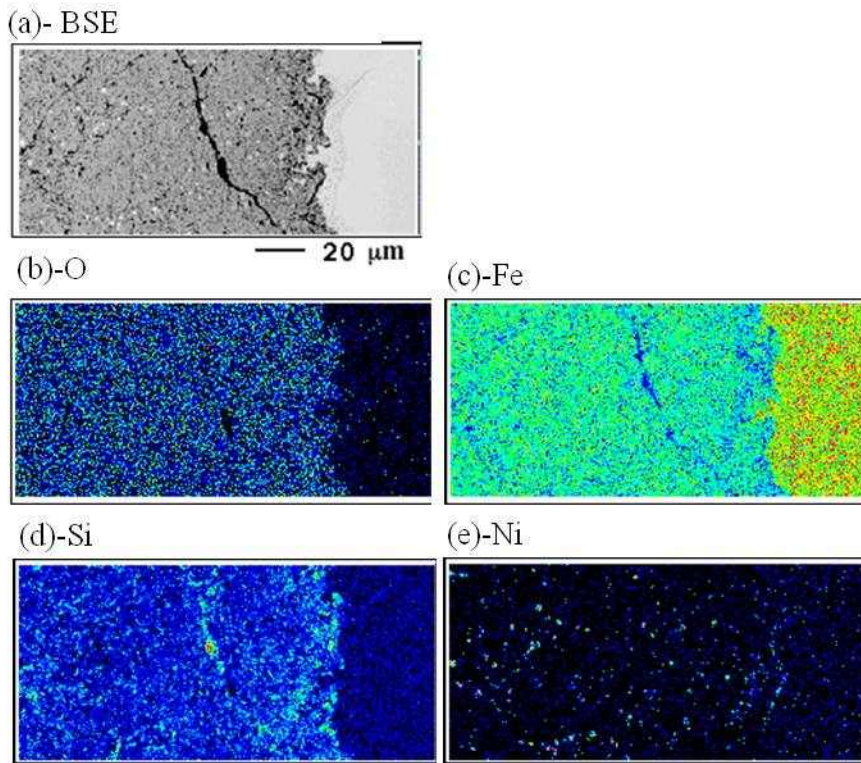FeO and dark part is Fe_2SiO_4 and white part is steel.

Fig. 5.4.9 EPMA images of oxides formed at 1000 ºC for 2 h of Ni Alloy;

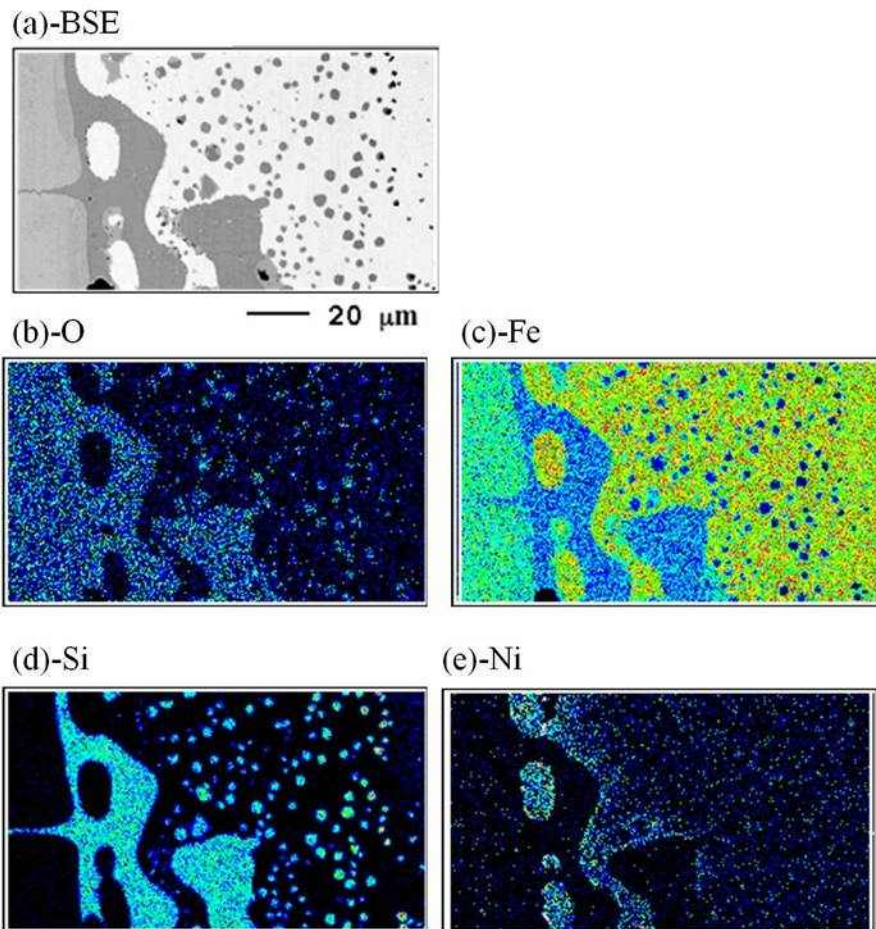(b), (c), (d) and (e) indicate O, Fe, Si, and Ni, respectively.

Fig. 5.4.10 EPMA images of oxides formed at 1250 ºC for 2 h of Ni Alloy;

(b), (c), (d) and (e) indicate O, Fe, Si, and Ni, respectively.

For Al Alloy, the interface became clean, however, the specific role of aluminum was not found clearly. Fig. 5.4.11 and Fig. 5.4.12 show BSE images of oxides formed on Al Alloy for 2 h at 1000 ºC and 1250 ºC respectively.
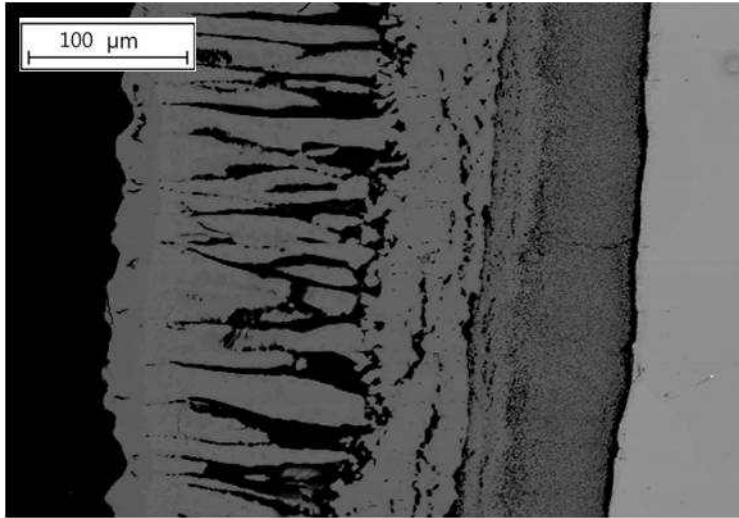
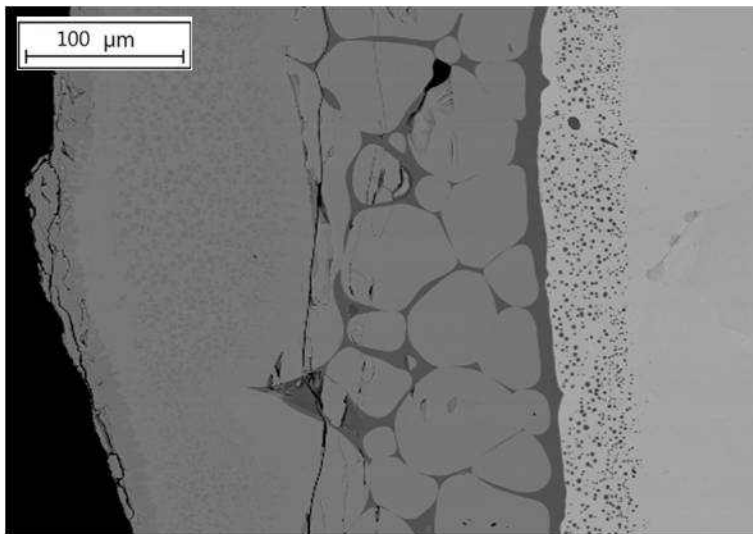Fig. 5.4.11. BSE images of oxides formed at 1000 ºC for 2 h of Al Alloy

Fig. 5.4.12. BSE images of oxides formed at 1250 ºC for 2 h of Al Alloy

Ⅵ Conclusions

The formation of red-scale in silicon added steel is caused by poor descalability of the primary scale due to the low melting temperature of fayalite. The aim of this study was to predict the formation of oxides so as to understand the red-scale formation and optimize the silicon concentration in steel. The formation of oxides of Fe – 0.1 C – (0 ~ 13) Si wt% steel at different temperatures was predicted with respect to the thermodynamics and kinetics. Also, the microstructures of oxides were analyzed by experimentally.

It was found that at high temperature, 1000 ℃ and 1250 ℃, FeO, SiO_2, Fe_2SiO_4 can be formed spontaneously on the silicon added steel in air. The most stable phase is SiO_2, however, it can change into Fe_2SiO_4 according to the partial pressure of oxygen.

Although the most stable phase is SiO_2 in air, most of the oxides formed on the Fe-Si consists of FeO. The thickness of oxides according to the time was calculated with respect to the diffusion of each elements. The growth of FeO is much faster than SiO_2, Fe_2SiO_4 because the diffusivity of Fe is greater than Si. To form SiO_2, silicon needs to diffuse more comparing with the formation of

Fe_2SiO_4 so SiO_2 cannot be formed. As increasing the silicon concentration from up to 13 wt%, the same phenomenon was predicted.

The oxides of silicon added steel were investigated experimentally. At 1000 ℃, the mixture of FeO and Fe_2SiO_4, the mixture of FeO and Fe_3O_4, Fe_3O_4, Fe_2O_3 were observed going from substrate to gas. At 1250 ℃, the eutectic compound of FeO and Fe_2SiO_4 the mixture of FeO and Fe_3O_4, Fe_3O_4, Fe_2O_3 were observed going from substrate to gas. The results were in a good agreement with the prediction because SiO_2 was not found and most of the oxides were composed of FeO.

The Effects of nickel and aluminum were investigated. It was found that the Ni addition (> 0.05 wt%) makes the interface between steel and oxides uneven because noble property and low diffusivity of Ni. If Al is added to the silicon containing steel, up to 0.5 wt%, it has no significant effect on SiO_2 or Fe_2SiO_4,

References

ABULUWEFA, H., GUTHRIE, R. & AJERSCH, F. 1996. The effect of oxygen concentration on the oxidation of low-carbon steel in the temperature range 1000 to 1250¡Æ C. Oxidation of Metals, 46, 423-440.

ADACHI, T. & MEIER, G. 1987. Oxidation of iron-silicon alloys. Oxidation of Metals, 27, 347-366.

AMANO, T., OKAZAKI, M., TAKEZAWA, Y., SHIINO, A., TAKEDA, M., ONISHI, T., SETO, K., OHKUBO, A. & SHISHIDO, T. Year. Hardness of oxide scales on Fe-Si alloys at room-and high-temperatures. In, 2006. Trans Tech Publ, 469-476.

ASAI, T., SOSHIRODA, T. & MIYAHARA, M. 1997. Influence of Ni impurity in steel on the removability of primary scale in hydraulic descaling. ISIJ international, 37, 272-277.

ATKINSON, A. 1982. A theoretical analysis of the oxidation of Fe---Si alloys. Corrosion Science, 22, 87-102.

BHADESHIA, H. 1999. Kinetics of Simultaneous Transformations. Proceedings of Solid-Solid Phase Transformations.

BHADESHIA, H., LORD, M. & SVENSSON, L. E. 2003. Silicon-Rich Bainite Steel Welds. Transactions of JWRI, 32, 43-52.

BIRKS, N., MEIER, G. H. & PETTIT, F. S. 2006. Introduction to the High-

temperature Oxidation of Metals, Cambridge Univ Pr.

BROWN, G. & WOLD, K. 1969. High-Temperature Oxidation of 0.14%C-3%Ni steel. J Iron Steel Inst, NOV.

CABALLERO, F., BHADESHIA, H., MAWELLA, K., JONES, D. & BROWN, P. 2001. Design of novel high strength bainitic steels: Part 1. Materials science and technology, 17, 512-516.

CABRERA, N. & MOTT, N. 1949. Theory of the oxidation of metals. Reports on progress in physics, 12, 163.

CHANG, Y. N. & WEI, F. I. 1989. High temperature oxidation of low alloy steels. Journal of Materials Science, 24, 14-22.

CHATTOPADHYAY, A. & CHANDA, T. 2008. Role of silicon on oxide morphology and pickling behaviour of automotive steels. Scripta Materialia, 58, 882-885.

CHEN, R. & YEUN, W. 2003. Review of the high-temperature oxidation of iron and carbon steels in air or oxygen. Oxidation of Metals, 59, 433-468.

CHEN, R. & YUEN, W. 2001. Oxide-scale structures formed on commercial hot-rolled steel strip and their formation mechanisms. Oxidation of Metals, 56, 89-118.

CHEN, W. & PETERSON, N. 1975. Effect of the deviation from stoichiometry on cation self-diffusion and isotope effect in wustite, $Fe_{1-x}O^*$ 1. Journal of Physics and Chemistry of Solids, 36, 1097-1103.

CHRISTIAN, J. W. 1975. The Theory of Transformations in Metals and Alloys. Pt. 1. Equilibrium and General Kinetic Theory. Pergamon Press, Oxford and New York. 1975, 586 p(Book).

DARKEN, L. S. & GURRY, R. 1945. The System Iron-Oxygen. I. The W stite Field and Related Equilibria. Journal of the American Chemical society, 67, 1398-1412.

DARKEN, L. S. & GURRY, R. W. 1946. The System Iron Oxygen. II. Equilibrium and Thermodynamics of Liquid Oxide and Other Phases. Journal of the American Chemical society, 68, 798-816.

DE COOMAN, B. 2004. Structure-properties relationship in TRIP steels containing carbide-free bainite. Current Opinion in Solid State and Materials Science, 8, 285-303.

DE COOMAN, B. C. 2007. Materials Design: The Key to Modern Steel Products, GRIPS Media GmbH.

FUKAGAWA, T., OKADA, H. & FUJIKAWA, H. 1997. Effect of P on hydraulic-descaling-ability in Si-added hot-rolled steel sheets. Tetsu-to-hagane, 83, 305-310.

FUKAGAWA, T., OKADA, H. & MAEHARA, Y. 1994. Mechanism of red scale defect formation in silicon-added hot-rolled steel sheets. ISIJ Int., 34, 906-911.

FUKAGAWA, T., OKADA, H., MAEHARA, Y. & FUJIKAWA, H. 1996. Effect of small amount of Ni on Hydraulic-descaling-ability in Si-added Hot-rolled

Steel Sheets. Journal of the Iron and Steel Institute of Japan-Tetsu to Hagane, 82**,** 63-68.

GARNAUD, G. & RAPP, R. A. 1977. Thickness of the oxide layers formed during the oxidation of iron. Oxidation of Metals, 11**,** 193-198.

GHOSH, G. & OLSON, G. 2002. Precipitation of paraequilibrium cementite: Experiments, and thermodynamic and kinetic modeling. Acta materialia, 50**,** 2099-2119.

GLEESON, B., HADAVI, S. & YOUNG, D. 2000. Isothermal transformation behavior of thermally-grown wustite. Materials at High Temperatures, 17**,** 311-319.

HARKINS, P. 1984. Dissolution of iron oxide under potential control.

JACQUES, P., GIRAULT, E., CATLIN, T., GEERLOFS, N., KOP, T., VAN DER ZWAAG, S. & DELANNAY, F. 1999. Bainite transformation of low carbon Mn-Si TRIP-assisted multiphase steels: influence of silicon content on cementite precipitation and austenite retention. Materials Science and Engineering A, 273**,** 475-479.

LEE, H. G. 1999. Chemical thermodynamics for metals and materials, Imperial College Press.

LEVIN, E. M., ROBBINS, C. R. & MCMURDIE, H. F. 1964. Phase diagrams for ceramists. BOOKS.

LOGANI, R. & SMELTZER, W. 1969. Kinetics of wustite-fayalite scale

formation on iron-silicon alloys. Oxidation of Metals, 1**,** 3-21.

LOGANI, R. & SMELTZER, W. 1971. The development of the wustite-fayalite scale on an iron-1.5 wt.% silicon alloy at 1000¡Æ C. Oxidation of Metals, 3**,** 15-32.

MATSUMURA, O., SAKUMA, Y. & TAKECHI, H. 1987. Enhancement of Elongation by Retained Austenite in Intercritical Annealed 0. 4 C--1. 5 Si--0. 8 Mn Steel. Trans. Iron Steel Inst. Jpn., 27**,** 570-579.

MILLOT, F. 1997. Diffusion of O18 in Fe3O4: An experimental approach to study the behavior of minority defects in oxides. Journal of Physics and Chemistry of Solids, 58**,** 63-72.

MORRIS, L. & SMELTZER, W. 1967. The kinetics of wustite scale formation on iron-nickel alloys. Acta Metallurgica, 15**,** 1591-1596.

MROWEC, S. 1967. On the mechanism of high temperature oxidation of metals and alloys. Corrosion Science, 7**,** 563-578.

OKADA, H., FUKUGAWA, T., ISHIHARA, H., OKAMOTO, A., AZUMA, M. & MATSUDA, Y. 1995. Prevention of red scale formation during hot rolling of steels. ISIJ Int.(Japan), 35**,** 886-891.

PAIDASSI, J. 1958. The Kinetics of the Oxidation of Iron in the Range 700-1250 C. Acta Metallurgica, 6**,** 184-194.

PALIN, G. 1965. Effect of heating conditions on the adhesion of the scale to the metal. STAL**,** 677-679.

PETTIT, F. & WAGNER JR, J. 1964. Transition from the linear to the parabolic rate law during the oxidation of iron to wustite in CO-CO2 mixtures. Acta Metallurgica, 12**,** 35-40.

POLLACK, H. W. 1977. Materials science and metallurgy, Reston Pub. Co.

RAMAN, R. 2006. Characterisation of [] rolled-in',[] fragmented'and [] red'scale formation during secondary processing of steels. Engineering Failure Analysis, 13**,** 1044-1050.

SACHS, K. & TUCK, C. 1968. Surface oxidation of steel in industrial furnaces. ISI publication**,** 1.

SAEGUSA, F. & LEE, L. 1966. Oxidation of Iron-aluminum Alloys In The Range 500 - 1000 C. Corrosion, 22**,** 168-177.

SHEPPARD, T. & STEEN, W. 1970. Hydraulic Descaling of Steel-A Preliminary Experimental Survey. J Iron Steel Inst., 208**,** 797-805.

STOTT, F. 1987. The protective action of oxide scales in gaseous environments at high temperature. Reports on progress in physics, 50**,** 861.

TANIGUCHI, S., YAMAMOTO, K., MEGUMI, D. & SHIBATA, T. 2001. Characteristics of scale/substrate interface area of Si-containing low-carbon steels at high temperatures. Materials Science and Engineering A, 308**,** 250-257.

TOFT, O. 1981. Nonstoichiometric Oxides. Academic Press, New York, NY.

TUCK, C. 1965. Non-protective and protective scaling of a commercial 1¨ú% silicon-iron alloy in the range 800 C-1000 C. Corrosion Science, 5**,** 631-643.

TUCK, C. & BARLOW, J. 1972. Effect of Reheating Furnace Atomosphere on The Adhesion of Scale to Steel. Iron Steel, 45**,** 31-38.

VIKTOROVICH, G., GUTIN, V. & LISOVSKLL, D. 1966. Solid-phase Equilibria of Wustite-iron Nickel Alloy. TSVETNYE MET**,** 47-49.

VIKTOROVICH, G. & LISOVSKII, D. 1966. Equilibrium of Solid Metal and Oxide in System Pe-Ni-O Soviet journal of non-ferrous metals, 7.

WAGNER, C. 1951. Diffusion and high temperature oxidation of metals. Atom Movements**,** 153-173.

WAGNER, C. 1956. Oxidation of alloys involving noble metals. Journal of the Electrochemical Society, 103**,** 571.

WULF, G., CARTER, T. & WALLWORK, G. 1969. The oxidation of FeNi alloys. Corrosion Science, 9**,** 689-701.

WYCKOFF, R. W. G. 1960. Crystal structures, Interscience publishers.

YUREK, G. J., HIRTH, J. P. & RAPP, R. A. 1974. The formation of two-phase layered scales on pure metals. Oxidation of Metals, 8**,** 265-281.

Acknowledgement

Curriculum Vitae

Name: Song, Eun-Ju

E-mail: joker12@postech.ac.kr

Date of birth: 28th December, 1985

Place of birth: Seoul, South Korea

Education

M. S. 2011, POSTECH (Pohang, Korea), Graduate Institute of Ferrous Technology, Computational Metallurgy Group

B. S. 2009, POSTECH (Pohang, Korea), Department of Mathematics